Supplementary Information (SI) for Journal of Materials Chemistry A. This journal is © The Royal Society of Chemistry 2025

### **Electronic Supplementary Information**

## Thermally polymerizable phthalocyanine realizes a metalnitrogen-doped carbon material featuring a defined single-atom catalyst motif with CO<sub>2</sub>RR activity

Yuki Sano<sup>a</sup>, Daichi Nakajima<sup>a</sup>, Biplab Manna<sup>b</sup>, Koki Chida<sup>c</sup>, Ryojun Toyoda<sup>\*a</sup>, Shinya Takaishi<sup>a</sup>, Kazuyuki iwase<sup>\*c</sup>, Koji Harano<sup>b,d</sup>, Yuta Nishina<sup>e,f</sup>, Takeharu Yoshii<sup>c</sup>, Ryota Sakamoto<sup>\*a, g</sup>

- Department of Chemistry, Graduate School of Science, Tohoku University, 6-3 AzaAoba,
  Aramaki, Sendai 980-8578, Japan
- Center for Basic Research on Materials, National Institute for Materials Science, 1-1
  Namiki, Tsukuba, Ibaraki 305-0044, Japan.
- Institute of Multidisciplinary Research for Advanced Materials, Tohoku University, 2-1-1
  Katahira, Aoba, Sendai, Miyagi, 980-8577, Japan.
- d. Research Center for Autonomous Systems Materialogy (ASMat), Institute of Integrated Research, Institute of Science Tokyo, 4259 Nagatsuda-cho, Midori-ku, Yokohama, Kanagawa 226–8501, Japan
- e. Graduate School of Natural Science and Technology, Okayama University. 3-1-1 Tsushimanaka, Kita-ku, Okayama 700-8530, Japan.
- f. Research Institute for Interdisciplinary Sciences, Okayama University. 3-1-1 Tsushimanaka, Kita-ku, Okayama 700-8530, Japan.
- g. Division for the Establishment of Frontier Sciences of Organization for Advanced Studies at Tohoku University, 2-1-1 Katahira, Aoba-ku, Sendai 980-8577, Japan.

#### **Experimental section**

#### **Materials**

All chemicals were purchased from commercial suppliers, and they were used without further purification.

#### Synthesis of 4-iodophenylboronic acid pinacol ester (1)

4-iodophenylboronic acid 2.478 g (10 mmol) and pinacol 1.241 g (10.5 mmol) were stirred in 50 mL of dry dichloromethane for 24 h at room temperature under a nitrogen atmosphere. The reaction solution was evaporated to obtain **2** as a white solid (yield: 98%).  $^{1}$ H NMR (Fig. S2; 500MHz, CDCl<sub>3</sub>)  $\delta$  7.72 (d, 2H),7.51 (d, 2H) 1.33 (s, 12H)

#### Synthesis of [4-(2-triisopropylsilylethynyl)phenyl]boronic acid (2)

**1** 3000 mg (9.09 mmol), CuI 86 mg (0.05 equiv), Pd(PPh<sub>3</sub>)<sub>2</sub>Cl<sub>2</sub> (0.05 equiv), and triisopropylsilylacetylene (1.25 equiv) were stirred in 50 mL of dry triethylamine for 24 h under nitrogen atmosphere. Then the reaction solution was filtered, and the filtrate was evaporated. The resulting solid was purified by column chromatography to obtain **2** as a white solid upon recrystallization with MeOH/H<sub>2</sub>O (yield: 68%). <sup>1</sup>H NMR (Fig. S3; 500MHz, CDCl<sub>3</sub>)  $\delta$  7.73 (d, 2H), 7.46 (d, 2H), 1.34 (s, 12H), 1.13 (s, 21H) <sup>13</sup>C NMR (Fig. S4; 125 MHz, CDCl<sub>3</sub>)  $\delta$ 11.44, 18.81, 25.00, 84.06, 92.16, 107.29, 126.35, 131.30, 134.58. The carbon directly bonded to boron could not be observed due to broadening caused by a shortened relaxation time resulting from cross-relaxation. MALDI-TOF-MS (Fig. S5) m/z calcd for C<sub>23</sub>H<sub>37</sub>N<sub>8</sub>BO<sub>2</sub>Si 407.25483, found 407.25481.

#### Synthesis of 4,5-bis[(4-triisopropylsilylethynyl)phenyl]phthalonitrile (3)

4,5-dichlorophthalonitrile 435 mg (2.21 mmol), **2** 2376 mg (6.18 mmol), Pd(PPh<sub>3</sub>)<sub>2</sub>Cl<sub>2</sub> 78 mg (0.05 eq) were stirred in 20 mL of dry 1,4-dioxane and saturated aqueous solution of K<sub>2</sub>CO<sub>3</sub> 1222 mg (8.84 mmol) for 24 h at 90 °C under a nitrogen atmosphere. After completion of the reaction, the reaction solution was filtered, and the filtrate was evaporated and extracted with dichloromethane. The solid was obtained by evaporation of dichloromethane purified by column chromatography and recrystallized with EtOH/H<sub>2</sub>O to give **3** as colorless needle-like crystals (yield: 78 %). <sup>1</sup>H NMR (Fig. S6; 500 MHz, CDCl<sub>3</sub>)  $\delta$  7.802 (s, 2H), 7.419 (d, 4H), 7.048 (d, 4H), 1.127 (s, 42H); <sup>13</sup>C NMR (Fig. S7; 125 MHz, CDCl<sub>3</sub>)  $\delta$  11.40, 18.79, 93.19, 106.09, 114.81, 115. 35, 124.25, 129.28, 132.58, 135.64, 137.27, 145.11.; MALDI-TOF-MS (Fig. S8) m/z calcd for C<sub>42</sub>H<sub>52</sub>N<sub>2</sub>Si<sub>2</sub> 663.35612, found 663.35615.

#### (triisopropylsilyl)ethynylphenyl]phthalocyaninatonickel (II) (4)

**3** 5393 mg (0.613 mmol), NiCl<sub>2</sub>·6H<sub>2</sub>O 38 mg (0.159 mmol) was added to 5 mL of 1-pentanol and 40  $\mu$ L of 1,8-Diazabicyclo[5.4.0]-7-undecene and stirred under nitrogen atmosphere at 160 °C for 24 hours. After completion of the reaction, the filtrate was evaporated, and the resulting solid was purified by column chromatography and reprecipitated with dichloromethane/methanol to afford **4** as a green solid (yield: 63 %). <sup>1</sup>H NMR (Fig. S9; 500 MHz, CDCl<sub>3</sub>)  $\delta$ 1.214 (s, 162H); <sup>13</sup>C NMR (Fig. S10; 125 MHz, CDCl<sub>3</sub>)  $\delta$  11.59, 18.95, 91.65, 107.26, 122.53, 123.97, 130.39, 132.24, 135.87, 141.34, 141.60, 145.64. ; MALDI-TOF-MS (Fig. S11) m/z calcd for C<sub>168</sub>H<sub>208</sub>N<sub>8</sub>NiSi<sub>8</sub> 2622.40628, found 2622.40783

# Synthesis of 2,3,9,10,16,17,23,24-octakis[4-ethynylphenyl]phthalocyaninatonickel (II) (Ni-OEPPc)

**4** 435 mg (0.166 mmol) of dehydrated THF (100 mL) solution in 8.3 mL (8.3 mmol) of 1 M THF solution of tetrabutylammonium fluoride was stirred dropwise under nitrogen atmosphere at −20 °C. After completion of the drop, the reaction solution was brought to room temperature and stirred for a further 48 hours. After completion of the reaction, the reaction solution was filtered through a 100 nm membrane filter paper, and the resulting solid was washed with chloroform and acetone to afford a dark green solid, **Ni-OEPPc**. (Yield: 88 %) IR (Fig. S12) (ATR) 3273 (C≡C-H) cm<sup>-1</sup>, 2099 (C≡C) cm<sup>-1</sup>; MALDI-TOF-MS (Fig. S13) (neg) m/z calcd for C36H12N6 [M+] 1371.33819, found 1371.33863.

#### Preparation of Ni-OEPPc/C

**Ni-OEPPc** (4 mg) and CNovel 010-00<sup>®</sup> (12 mg) were combined with 5 mL of dehydrated THF and subjected to ultrasonication for 10 minutes. THF was then removed using a rotary evaporator. After solvent removal, the sample was stored in a vacuum oven at 80 °C for over 24 hours before use.

#### Characterization

<sup>1</sup>H and <sup>13</sup>C NMR measurements were performed on a Bruker AV500. MALDI-TOF-MS for **2**, **3**, **4**, and **Ni-OEPPc** were performed on JMS-T100GCV at Research and Analytical Center for Giant Molecules Section of Analysis Research (Graduate School of Science, Tohoku University). TG-DTA was conducted on a DTG-60H (Shimadzu) with a heating rate of 10 °C min<sup>-1</sup> under Ar flow (100 mL min<sup>-1</sup>). <sup>13</sup>C DD-MAS solid NMR spectra were measured on an JEOL ECZL-400 (100 MHz) at Technical Division, School of Engineering, Tohoku University. The thermal decomposition behavior of **Ni-OEPPc** were assessed by simultaneous analysis systems including thermogravimetry, differential scanning calorimetry,

and mass spectroscopy (TG-DSC-MS). TG-DSC was conducted on a STA 449 Jupiter (Netzsch) from 60 °C to 800 °C at a heating rate of 10 °C min<sup>-1</sup> under a He flow (150 mL min<sup>-1</sup> 1). The emission gas from TG-DSC was analysed by using a quadrupole mass spectrometer (JMS-Q1500GC, JEOL). FT-IR spectra were acquired using a Jasco FT/IR-4200 spectrometer. Therein, an attenuated total refraction (ATR) attachment with a ZnSe window was used. Raman spectra were obtained on LabRAM HR resolution (HORIBA) with the laser wavelength of 633 nm. Electrical conductivities were measured with two electrode configurations at 300 K using an Agilent E5291A SMU module installed in an E5260A mainframe. Therein samples were prepared by making compressed pellets of 3 mm diameter by applying 250 kgw. The channel length was 0.060 cm. X-ray photoelectron spectroscopy (XPS) analysis of the materials was performed with a basic chamber pressure of < 1×10<sup>-6</sup> Pa with an anode using Mg K $\alpha$  radiation (hu = 1253.6 eV) with 12 kV and 25 mA. XPS deconvolution was conducted with CasaXPS. The binding energy of all elements was calibrated by using the C1s peak at 284.8 eV as a reference<sup>1</sup>. The deconvolution of N 1s peaks was conducted according to the literatures<sup>2,3</sup>. Ni K-edge X-ray absorption spectroscopy (XAS) measurements were performed on the BL01B1 and BL14B2 beamlines at SPring-8 of the Japan Synchrotron Radiation Research Institute (JASRI). A double-crystal Si(111) monochromator and transmission mode were employed for the measurements. The first peak maximum in the Cu foil spectrum was set to 8980.3 eV for calibration of the energy levels. Data reduction, data analysis, and EXAFS fitting were performed and analyzed with the Athena and Artemis programs of the Demeter data analysis packages4. Powder X-ray diffraction patterns were collected on a Rigaku SmartLab with Cu K $\alpha$  radiation ( $\lambda$  = 1.5406 Å) at room temperature. Transmission electron microscopy (TEM), high-angle annular dark-field (HAADF) scanning transmission electron microscopy (STEM) imaging and energy-dispersive spectroscopy (EDS) analysis were carried out on a Thermo Fisher Scientific Talos F200X G2 equipped with an EDS detector (Super-X G2) at an acceleration voltage of 80 kV. The specimens for TEM were prepared by depositing ethanol dispersion of Ni-OEPPc/C or Ni-OEPPc/C\_700 onto a TEM copper grid with a lacy carbon support (NS-C15, Okenshoji Co., Ltd.). A probe current for HAADF-STEM and EDS mapping was set to ca. 500 pA. Analysis of EDS spectrum imaging was carried out on Velox software (Thermo Fisher Scientific) using a single three-parameter Bethe-Heitler function as a background correction parameter. N2 adsorption/desorption isotherms were measured at 77 K on BELSORP-MAX2 (MicrotracBEL). Specific surface areas were calculated by the Brunauer-Emmett-Teller (BET) method in the pressure range of P/P0 = 0.05-0.35. The pore-size distribution was calculated with the non-local density functional theory (NLDFT) with a slit-pore model using BELMaster. Samples for DLS were prepared by adding 5 mL of THF to 4 mg of Ni-OEPPc. Particle size distribution analysis was performed by the Marquardt method using the software appended in DLSZneo. Thermal treatment was carried out on VF-3000A (SK medical) with a heating rate of 10 °C min<sup>-1</sup> under Ar flow (100 mL min<sup>-1</sup>). ICP was measured by ICPE-9820 (Shimadzu) at Research and Analytical Center for Giant Molecules Section of Analysis Research (Graduate School of Science, Tohoku University).

#### **Electrochemical measurement**

CO<sub>2</sub>RR activity were evaluated using an HZ-7000 potentiostat (Hokuto Denko) equipped with a HZAP3003A booster (Hokuto Denko). Custom-made three compartment electrochemical cells, in which the anodic and cathodic compartments were separated by a Nafion membrane (Nafion 117, Sigma-Aldrich), were employed for the measurements. The catalysts' loaded GDEs were fabricated by spraying the catalysts' inks onto the commercially available GDEs (MFK-A, Mitsubishi Chemical) using an airbrush (Anest Iwata Eclipse HP-BS). The catalyst inks were prepared by ultrasonication of a mixture containing 3 mg of catalysts, 300 µL of ethanol, and 10 µL of 5 wt% Nafion solution (Wako, polymer content: 5.0-5.4%). Catalystloaded GDEs, Ag/AgCl (in a saturated KCl solution), and carbon paper loaded with IrO2 (Tanaka Precious Metals, TEM77100(SA100)) were employed as the working, reference, and counter electrodes, respectively. The geometric surface area of each working electrode was 1.89 cm<sup>2</sup>. In long-term measurement beyond 4 hours, the catalyst ink was prepared by ultrasonication of a mixture containing 3 mg of catalysts, 300 µL of ethanol, 50 µL of 5 wt% Nafion solution (Wako, polymer content: 5.0-5.4%), and 200 µL of 1 wt% PTFE solution (AGC Chemicals). Then, 350 µL of the resulting ink was sprayed onto the surface of GDE. Potassium bicarbonate (KHCO<sub>3</sub>, Sigma-Aldrich, ACS reagent, 99.7%) was used to prepare the electrolyte. Gaseous CO<sub>2</sub> (Taiyo Nippon Sanso, 99.995%) was fed to the gas phase compartment at a flow rate of 10 mL min<sup>-1</sup> using a mass flow controller. The CO₂RR products were analyzed after 30 min of constant current electrolysis for evaluation of CO<sub>2</sub>RR activity. The potentials of the working electrodes are presented on the reversible hydrogen electrode (RHE) scale, and all measurements were iR-corrected. Gas phase products were captured using a gasbag and quantitatively analyzed with a gas chromatograph (GC-2014, Shimadzu) equipped with a thermal conductivity detector to analyze H2 and a flame ionization detector with a methanizer (MTN-1, Shimadzu) to analyze CO. Liquid products were analyzed using 1H nuclear magnetic resonance spectroscopy (NMR) with a pre-saturation method reported elsewhere using dimethyl sulfoxide (Wako) as an internal standard., employing an AVANCE III 600 (Bruker).

Cyclic voltammograms (CVs) were acquired by using a custom-made single-compartment cell with a three-electrode system. The catalyst inks were prepared ultrasonication of a

mixture containing 3 mg of catalysts, 300 μL of ethanol, and 10 μL of a 5 wt % Nafion solution (Wako, polymer content: 5.0–5.4%). 7.5 μL of the catalyst ink was drop-cast onto the glassy carbon rotation disk electrodes and air-dried. This electrode was then used as the working electrode. In each trial, a catalyst-loaded glassy carbon (Pine, electrode area: 0.20 cm²), Ag/AgCl (saturated KCl solution), and carbon rod were employed as the working, reference, and counter electrodes, respectively. A 1 M KHCO<sub>3</sub> solution saturated with CO<sub>2</sub> or a 1 M phosphate buffered solution, that were prepared using sodium dihydrogen phosphate (NaH<sub>2</sub>PO<sub>4</sub>, Wako, Guaranteed Reagent) and disodium hydrogen phosphate (Na<sub>2</sub>HPO<sub>4</sub>, Wako, Guaranteed Reagent), saturated with Ar was used as the electrolyte. The solution pH was adjusted to 7.9 in each case. The scan rate was 50 mV s<sup>-1</sup>. The potentials of the working electrodes are presented on the reversible hydrogen electrode (RHE) scale, and all measurements were iR-corrected.

The electrochemically active surface area (ECSA) was evaluated using cyclic voltammetry (CV) in 0.1 M KOH. Multiple CV scans were performed in the non-Faradaic region at various scan rates (10, 15, 20, 25, and 30 mV s<sup>-1</sup>). The double-layer capacitance (C<sub>dl</sub>) was estimated from the slope of the linear fit between the current density and the scan rate. The ECSA was then calculated using the following equation:

$$ECSA (cm^2) = \frac{C_{dl}}{C_s}$$

where  $C_s$  represents the specific capacitance per unit area. In this study, a commonly accepted value of 0.040 mF cm<sup>-2</sup> was used for  $C_s^{5,6}$ .

Furthermore, based on the estimated ECSA, the mass-specific ECSA and specific activity were calculated using the following equations:

Specific activity 
$$(A cm^{-2}) = \frac{I_{CO}}{ECSA}$$

Mass specific ECSA (cm<sup>2</sup> g<sup>-1</sup>) = 
$$\frac{ECSA}{m_{cat}}$$

where m<sub>cat</sub> is the mass of the catalyst, and I<sub>CO</sub> is the partial current for CO production.

The Faraday efficiency of a certain gas product was calculated according to the following equation:

$$FE (\%) = \frac{nFxV}{jAt}$$

where n (= 2) is the number of electrons required to form one molecule of CO, F is Faraday's constant (96,485 C mol<sup>-1</sup>), x is the concentration (mol L<sup>-1</sup>) of the gaseous product, V is the total volume of the collected gas, and j is the current density applied during the CO<sub>2</sub> reduction reaction, A is the geometric electrode area, and t is the time for the electrolysis.

The TOF for CO production was calculated according to the following equation:

$$TOF(s^{-1}) = \frac{j_{co}/nF}{m_{cat} \times \alpha/M_{metal}}$$

where the  $j_{CO}$  is the partial current density for CO, n is the number of electrons transferred for CO, F is the Faradaic constant (96485 C mol<sup>-1</sup>), m<sub>cat</sub> is the catalyst mass in the electrode (g),  $\alpha$  is the Ni content in the catalysts measured by ICP, and M<sub>metal</sub> is the atomic mass of metal.

The mass activity was calculated according to the following equation:

Mass activity (mA 
$$mg^{-1}$$
) =  $\frac{j_{co}}{m_{cat} \times \alpha}$ 

where the  $j_{CO}$  is the partial current density for CO (mA),  $m_{cat}$  is the catalyst mass in the electrode (mg),  $\alpha$  is the Ni content in the catalysts measured by ICP (wt%).

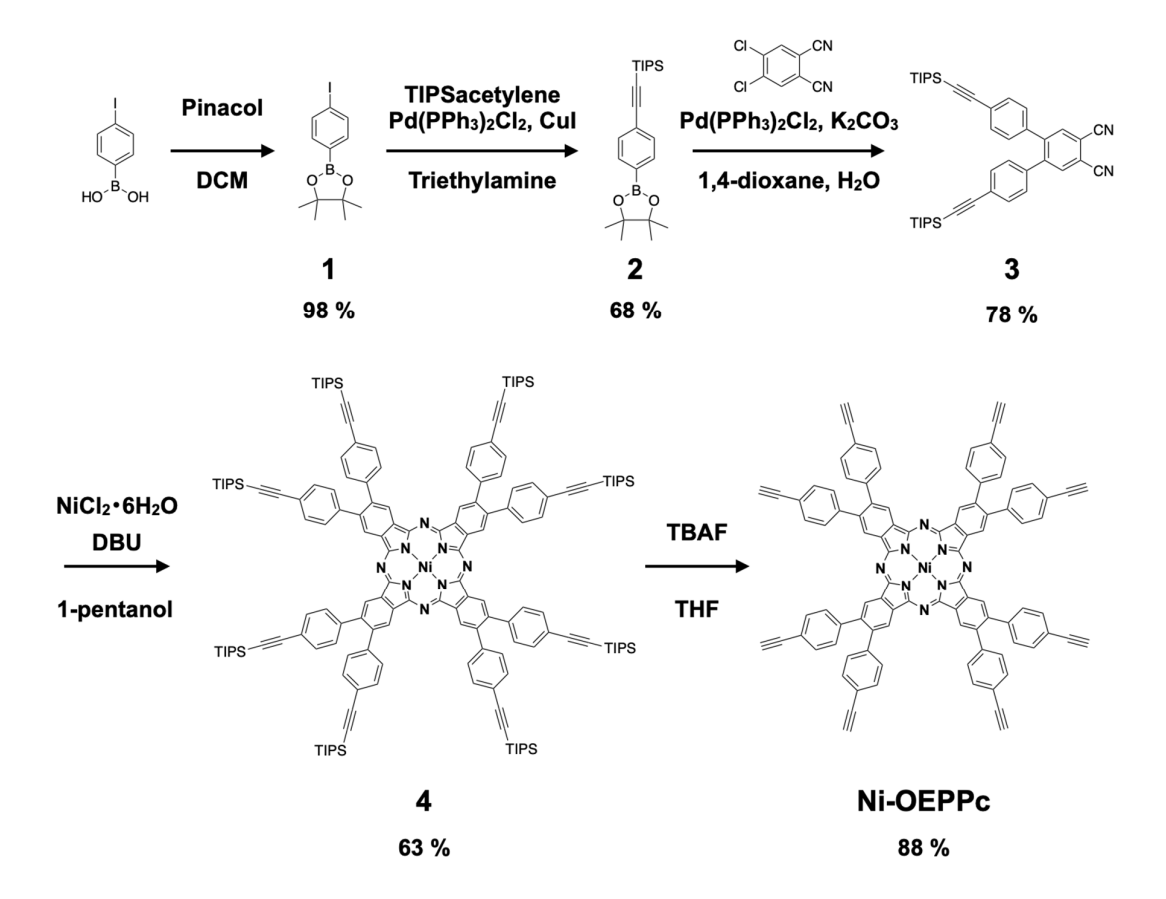


Fig. S1 Synthetic scheme of Ni-OEPPc.

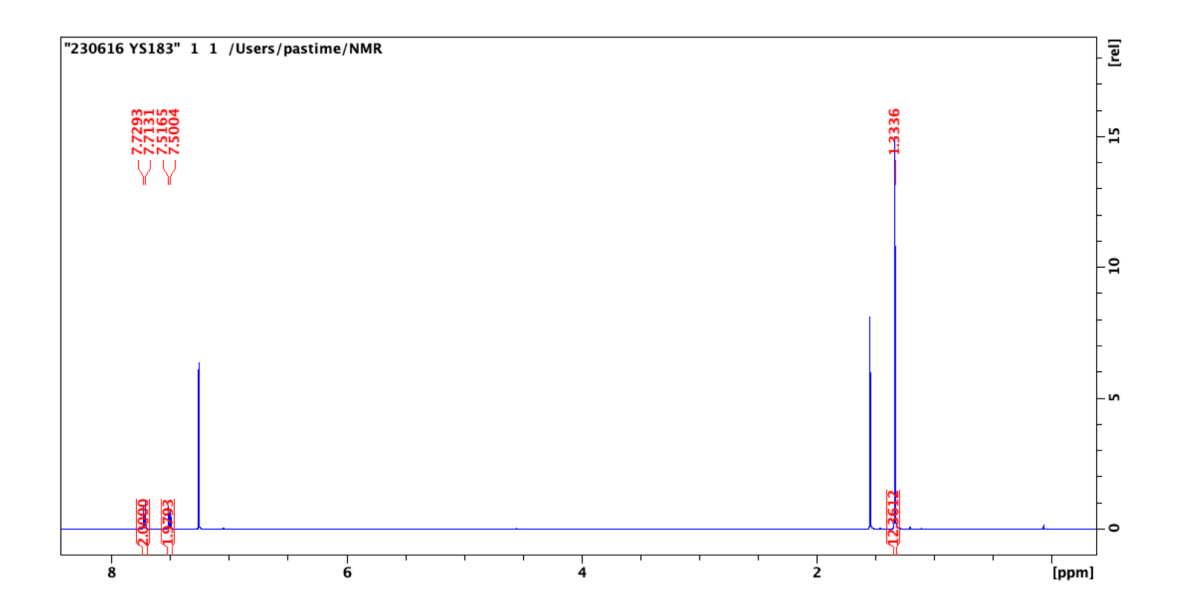


Fig. S2 <sup>1</sup>H NMR spectrum of 1 in chloroform-d.

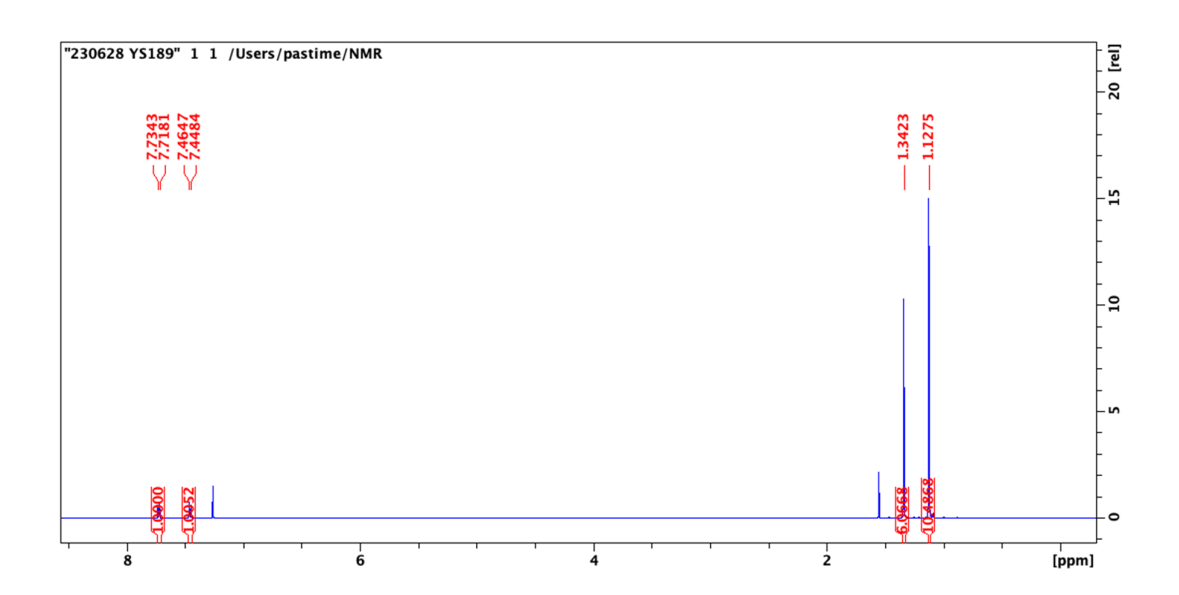


Fig. S3 <sup>1</sup>H NMR spectrum of 2 in chloroform-d.

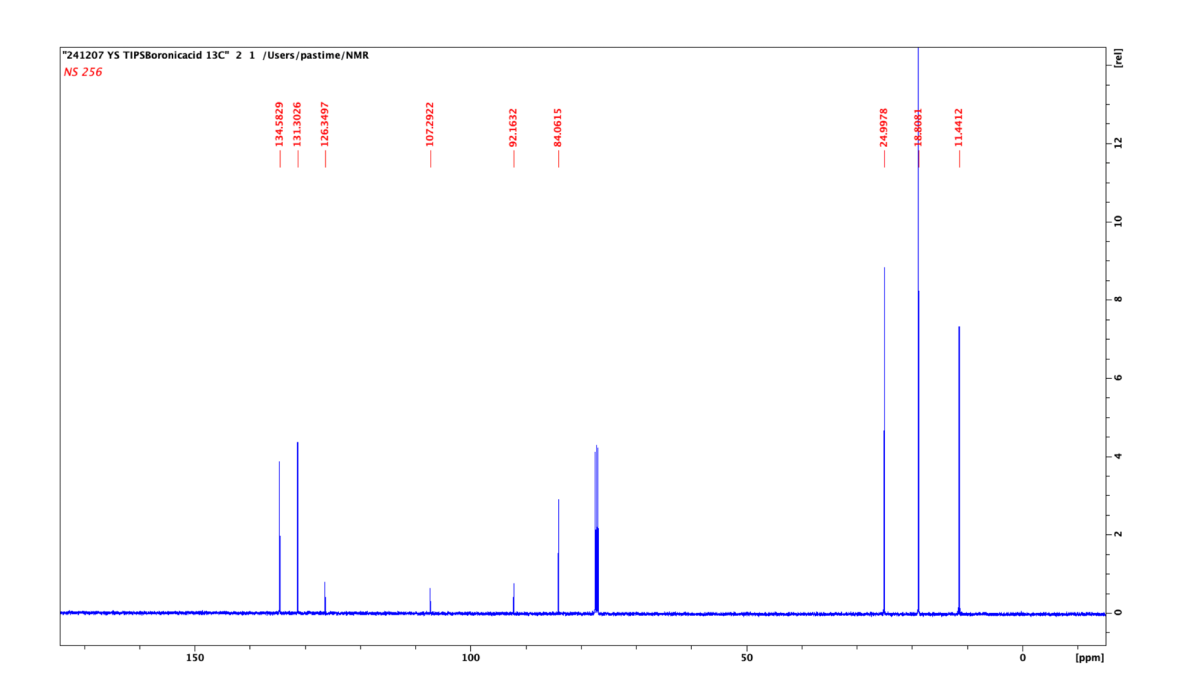


Fig. S4 <sup>13</sup>C NMR spectrum of 2 in chloroform-d.

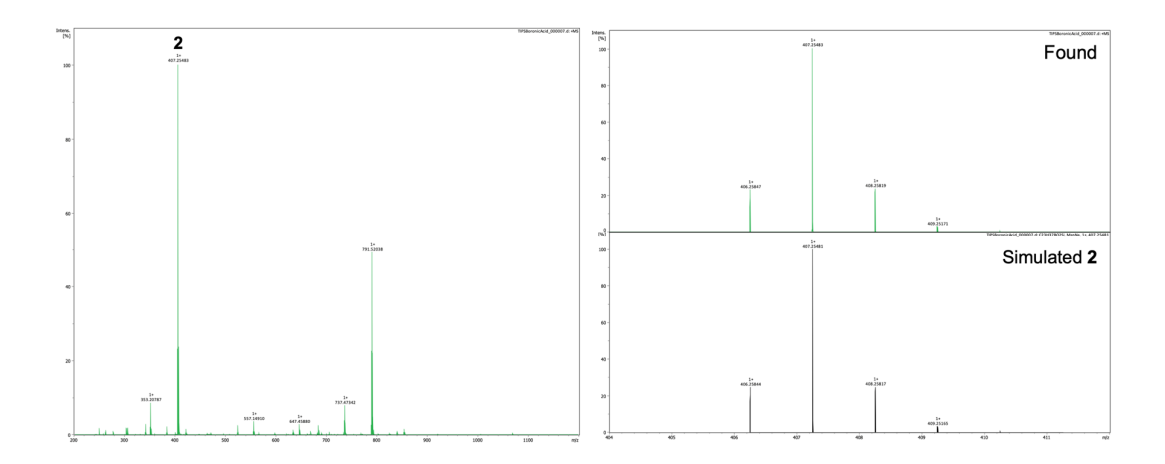


Fig. S5 Experimental and simulated MALDI-TOF-MS for 2.

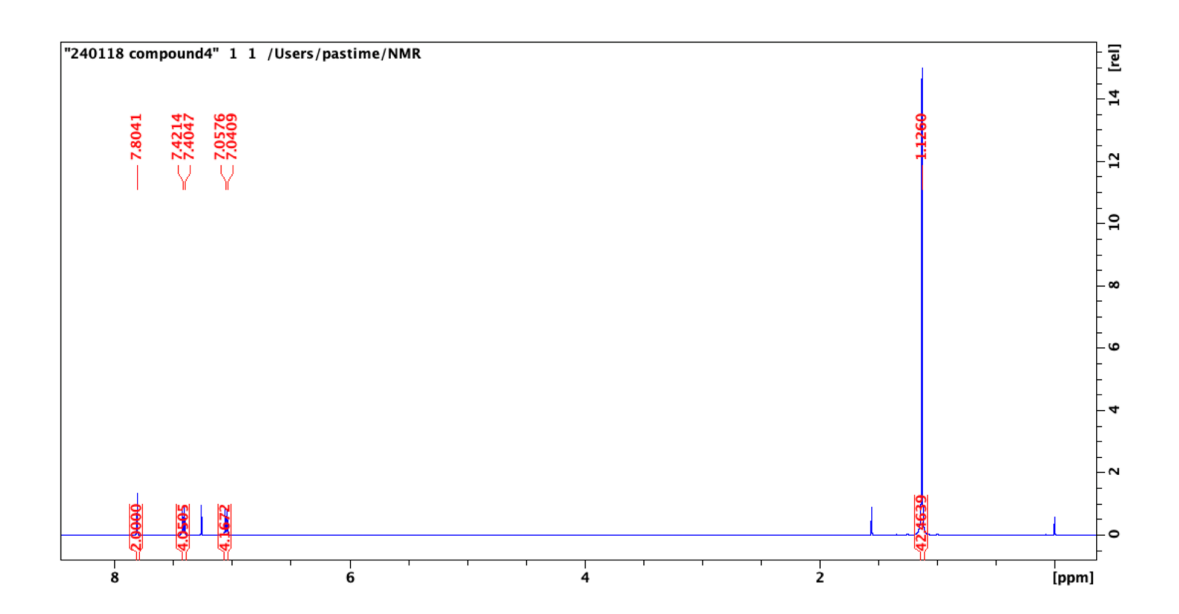


Fig. S6 <sup>1</sup>H NMR spectrum of 3 in chloroform-d.

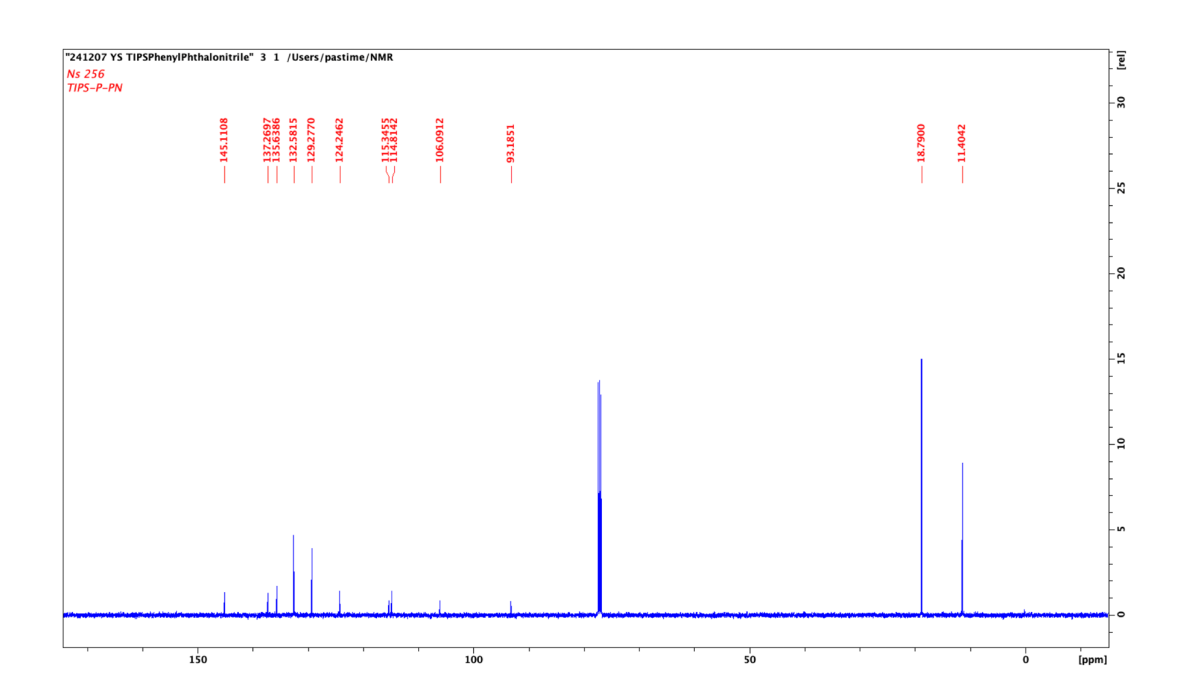


Fig. S7 <sup>13</sup>C NMR spectrum of 3 in chloroform-d.

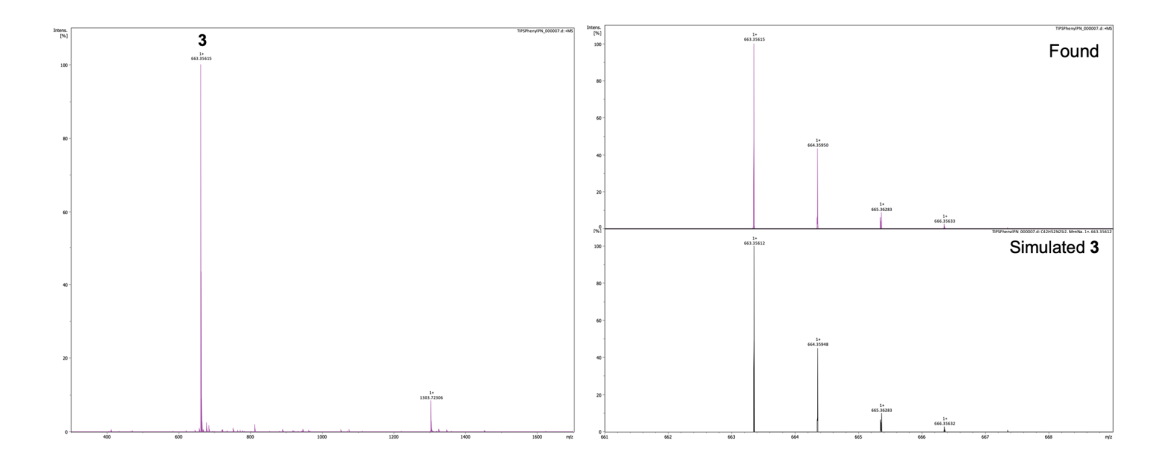


Fig. S8 Experimental and simulated MALDI-TOF-MS for 3.

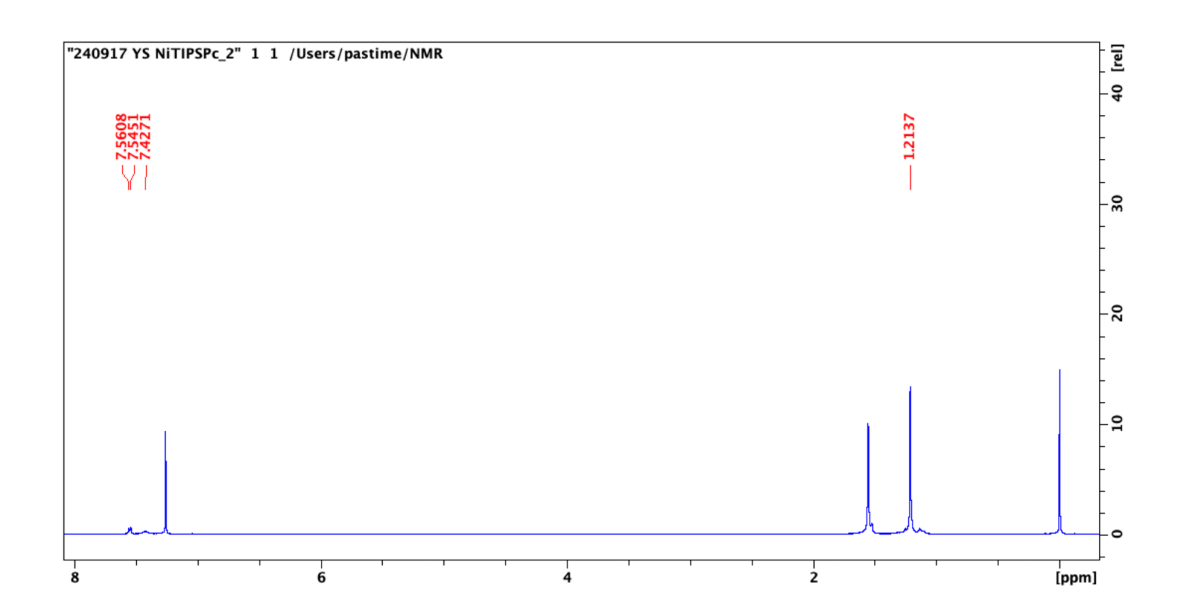


Fig. S9 <sup>1</sup>H NMR spectrum of 4 in chloroform-d.

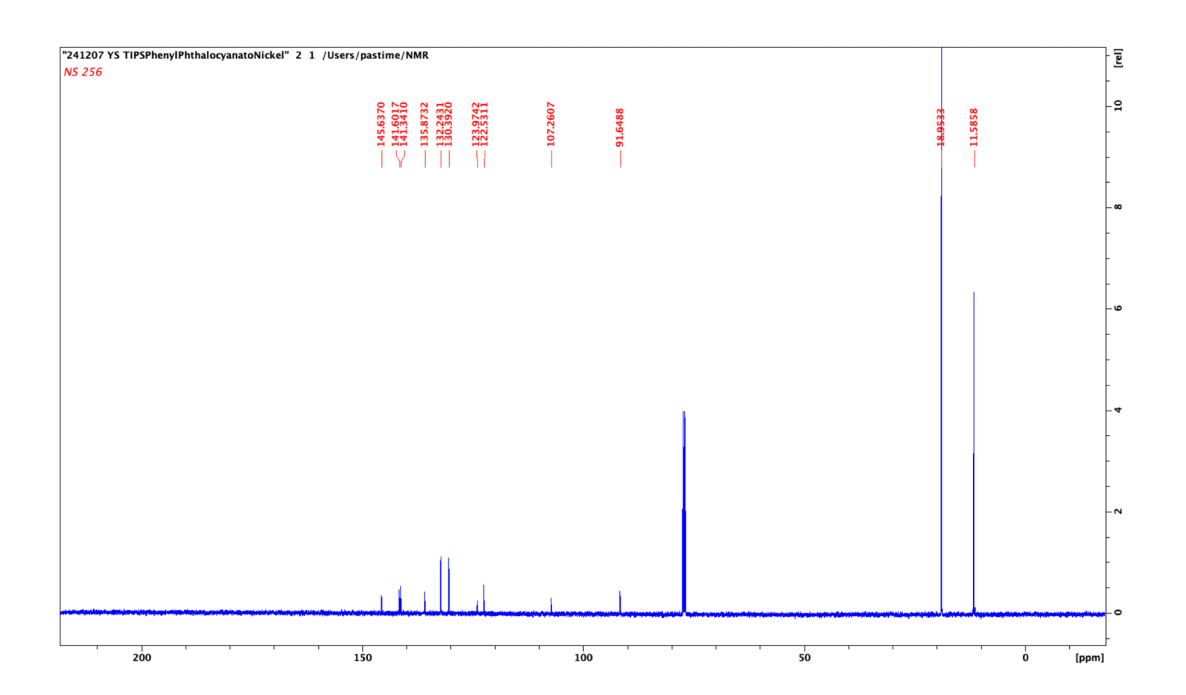


Fig. S10 <sup>13</sup>C NMR spectrum of 4 in chloroform-d.

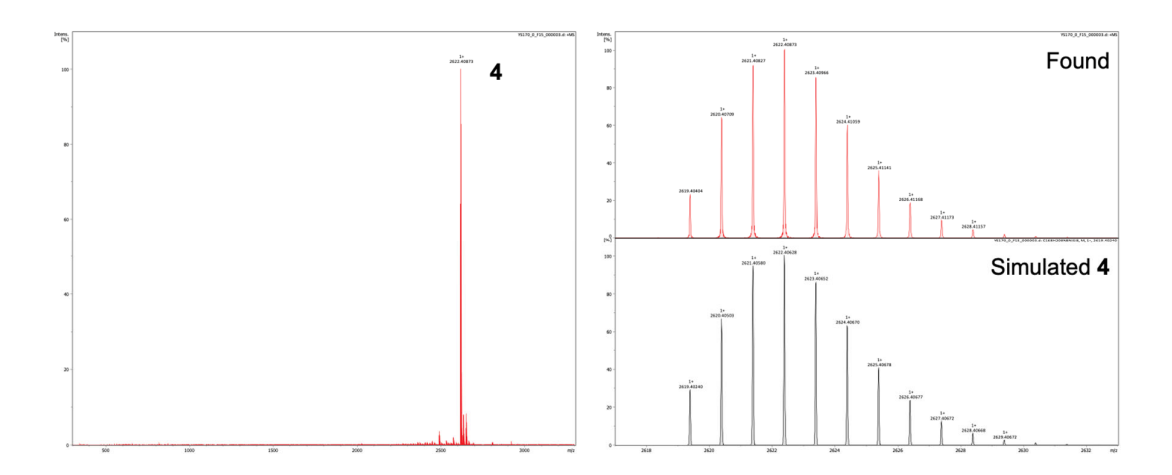


Fig. S11 Experimental and simulated MALDI-TOF-MS for 4.

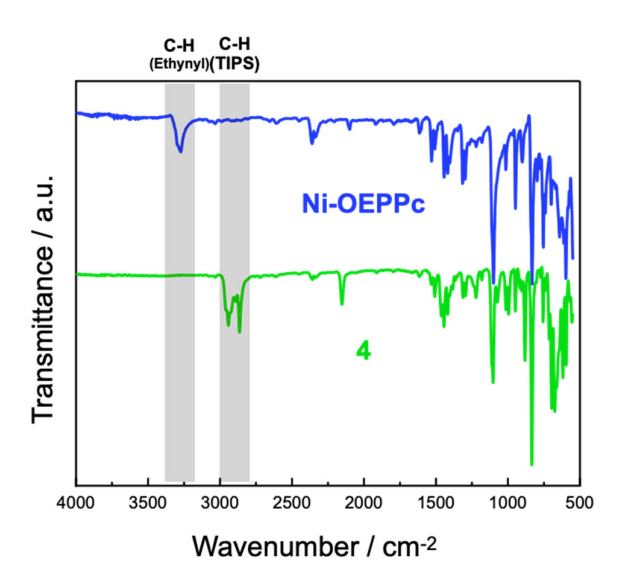


Fig. S12 IR spectra of Ni-OEPPc and 4.

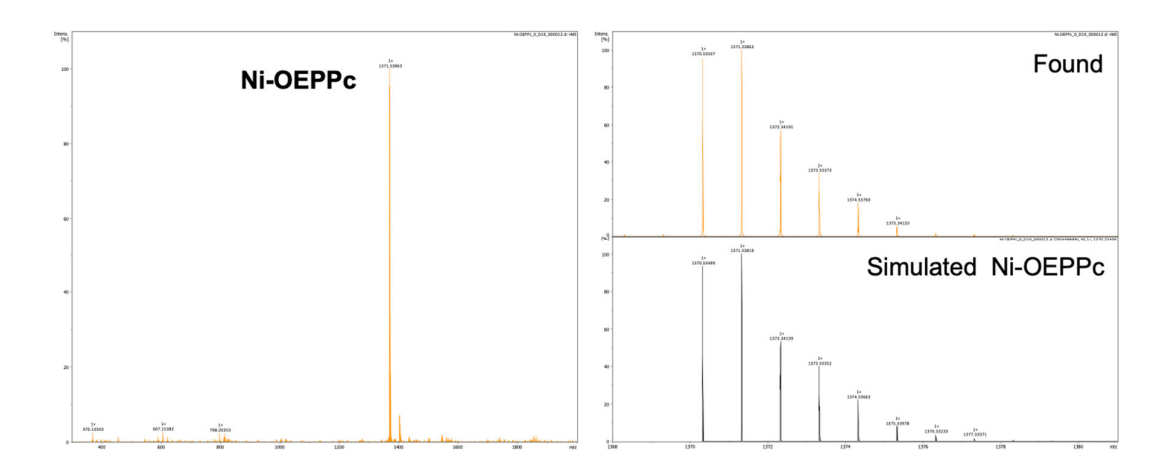


Fig. S13 Experimental and simulated MALDI-TOF-MS for Ni-OEPPc.

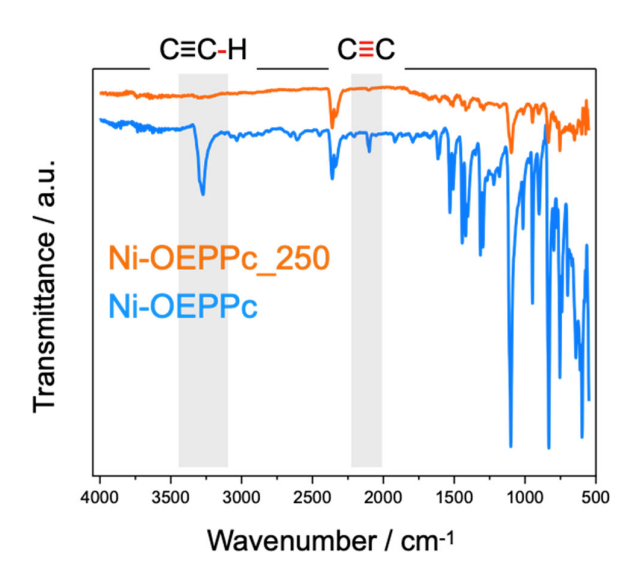


Fig. S14 IR spectra of Ni-OEPPc and Ni-OEPPc\_250.

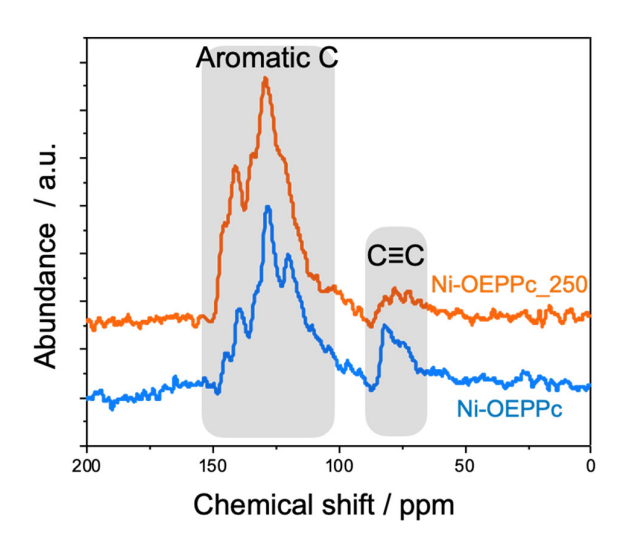


Fig. S15 Solid-state  $^{13}\text{C}$  NMR spectra of Ni-OEPPc and Ni-OEPPc\_250.

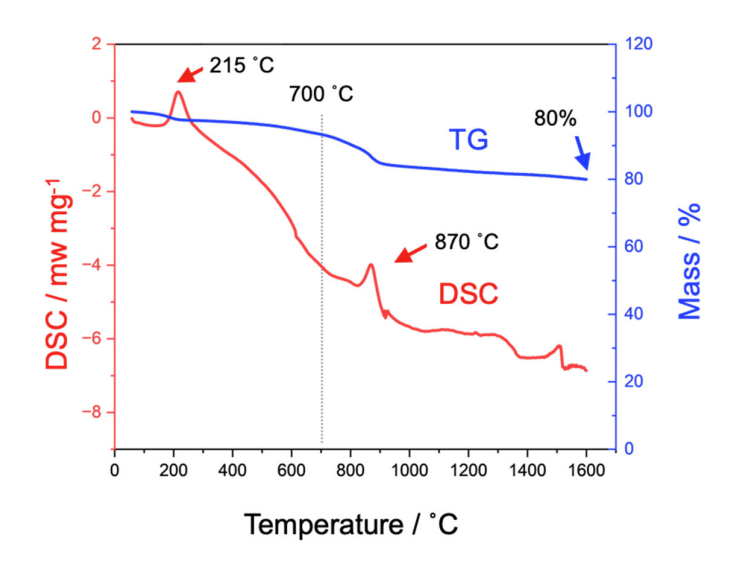


Fig. S16 TG-DSC curves of Ni-OEPPc up to 1600 °C.

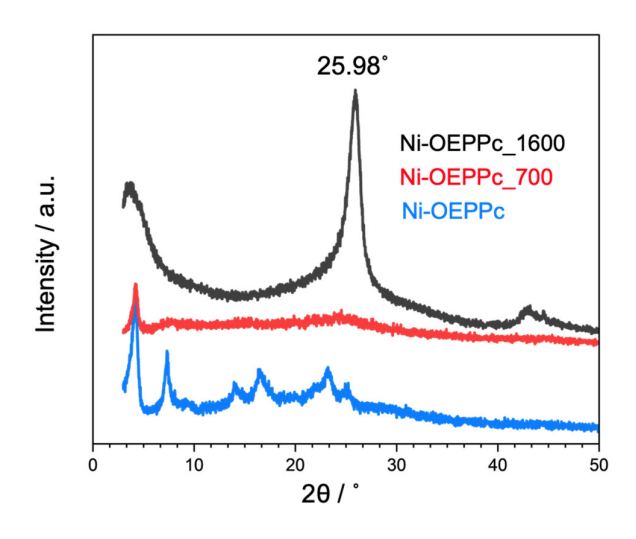


Fig. S17 PXRD patterns of Ni-OEPPc, Ni-OEPPc\_700, and Ni-OEPPc\_1600.

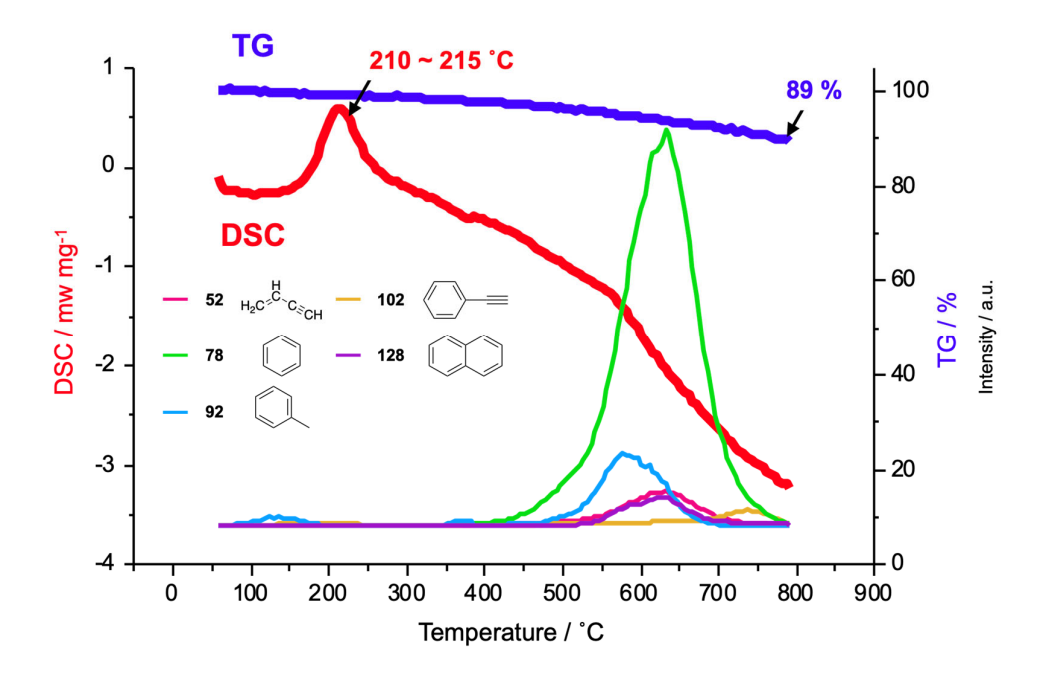


Fig. S18 TG-DSC-Mass for Ni-OEPPc.

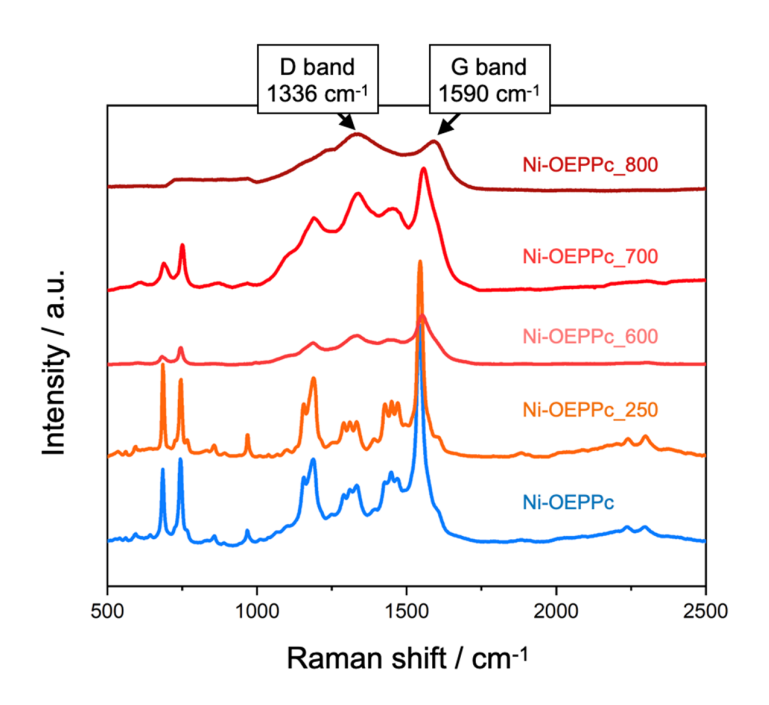


Fig. S19 Raman spectra of Ni-OEPPc, Ni-OEPPc\_250, Ni-OEPPc\_600, Ni-OEPPc\_700, and Ni-OEPPc\_800.

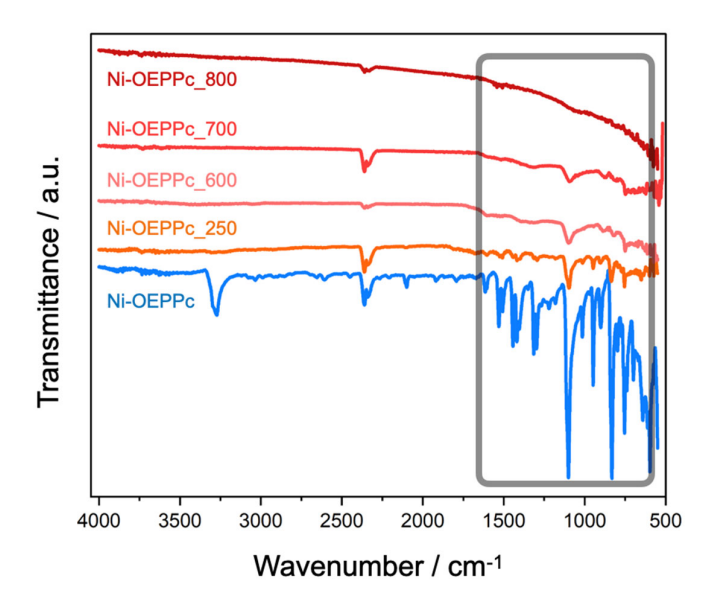
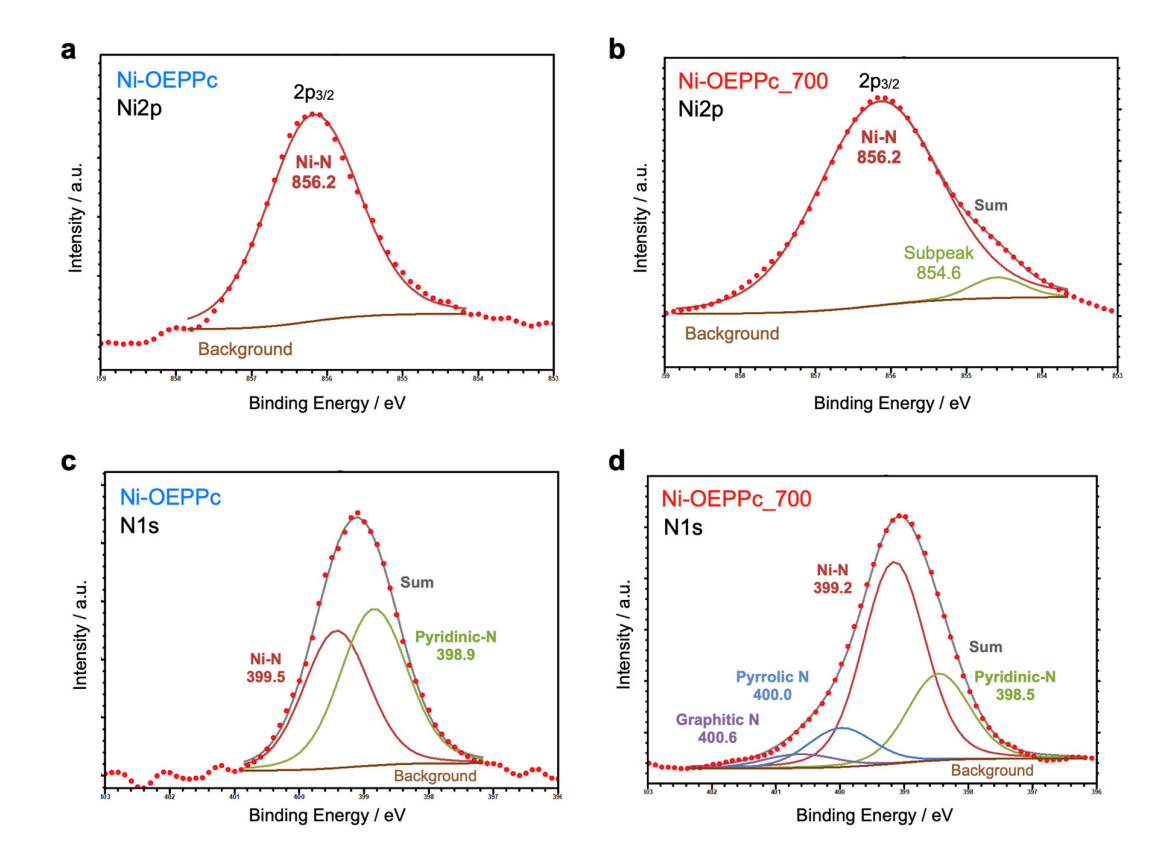


Fig. S20 IR spectra of Ni-OEPPc, Ni-OEPPc\_250, Ni-OEPPc\_600, Ni-OEPPc\_700, and Ni-OEPPc\_800.



**Fig. S21** (a-d) N 1s and Ni 2p<sub>3/2</sub> XP spectra of **Ni-OEPPc** and **Ni-OEPPc\_700**. The subpeak observed in (b) is ascribed to the negligible amount of oxidized Ni species, carbides, or metallic Ni.<sup>7</sup>

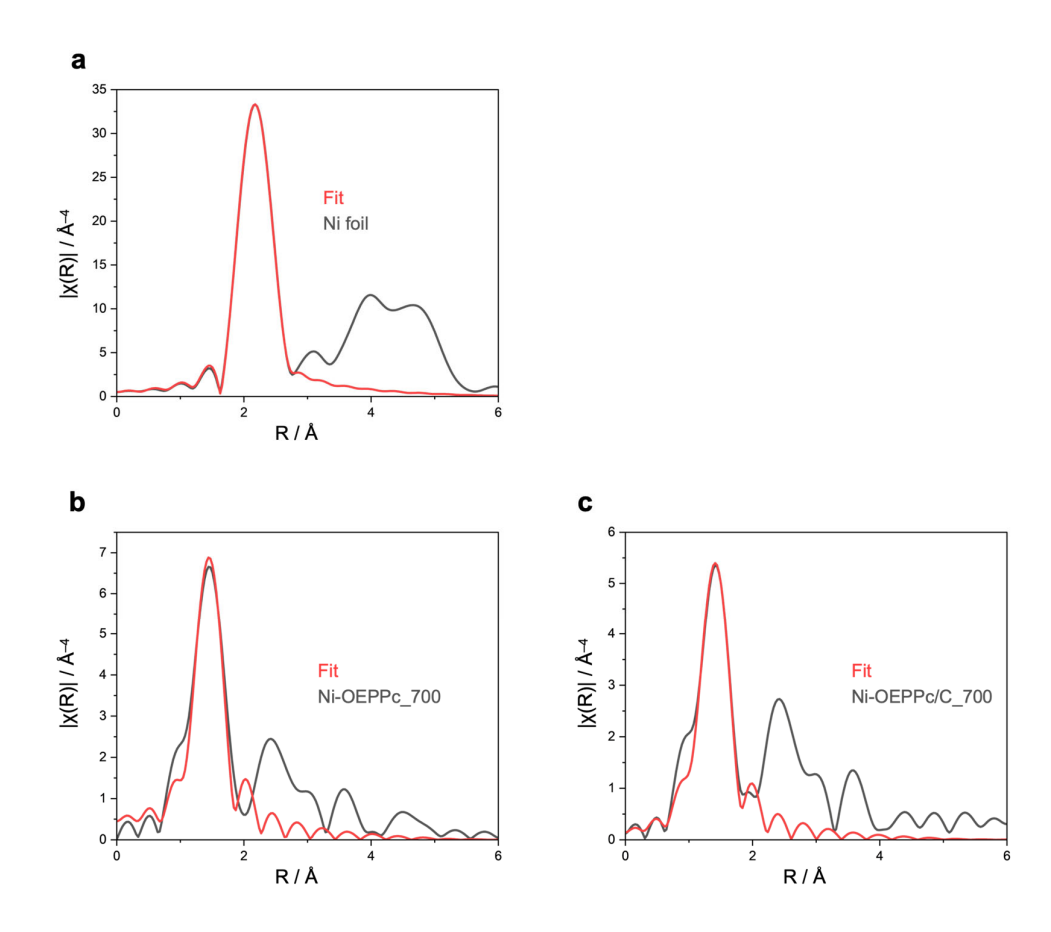
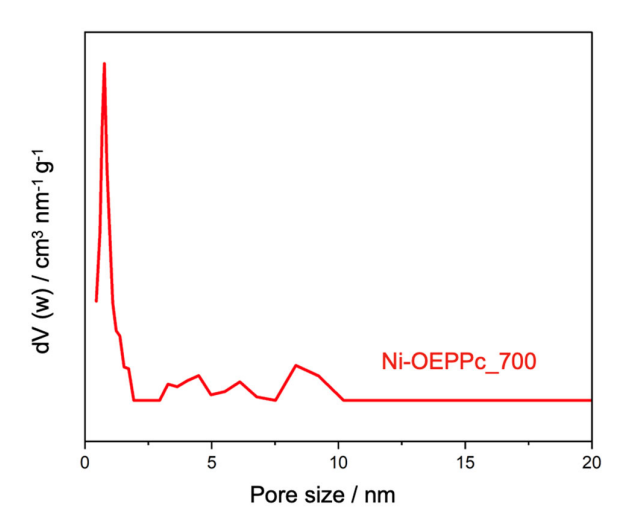
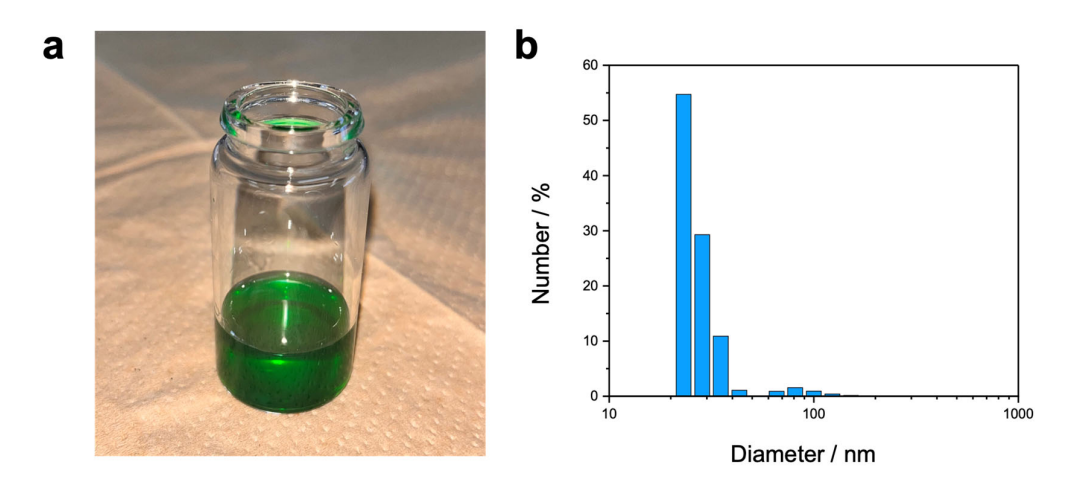


Fig. S22 R-space fitting of EXAFS spectra for (a) Ni foil, (b) Ni-OEPPc\_700, and (c) Ni-OEPPc/C\_700.



 $\textbf{Fig. S23} \ \ \text{Pore size distribution calculated using the NLDFT method for } \textbf{Ni-OEPPc\_700}.$ 



**Fig. S24** (a) Photograph of **Ni-OEPPc** dispersion in THF. (b) Particle size distribution of **Ni-OEPPc** dispersed in THF by DLS.

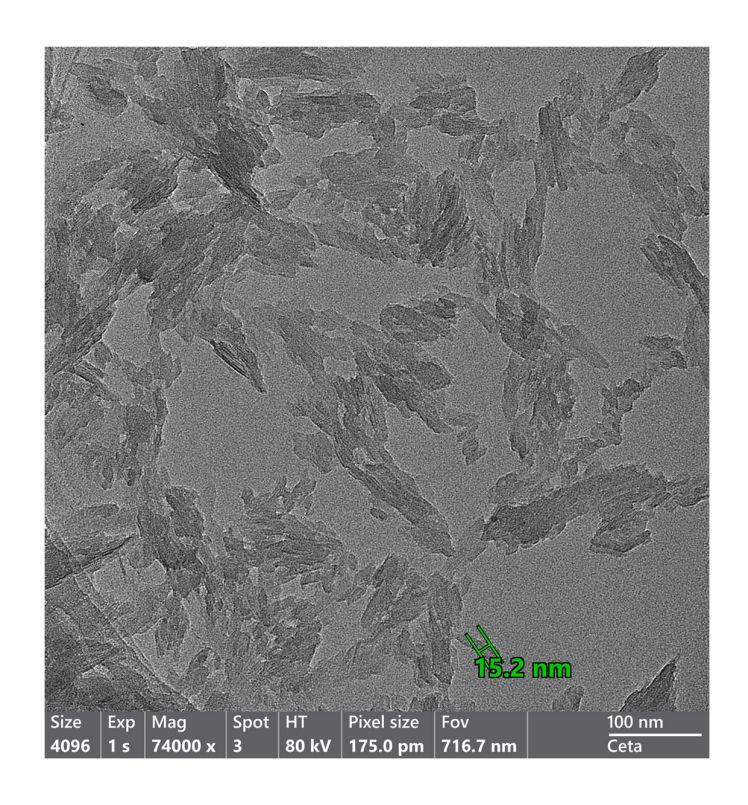
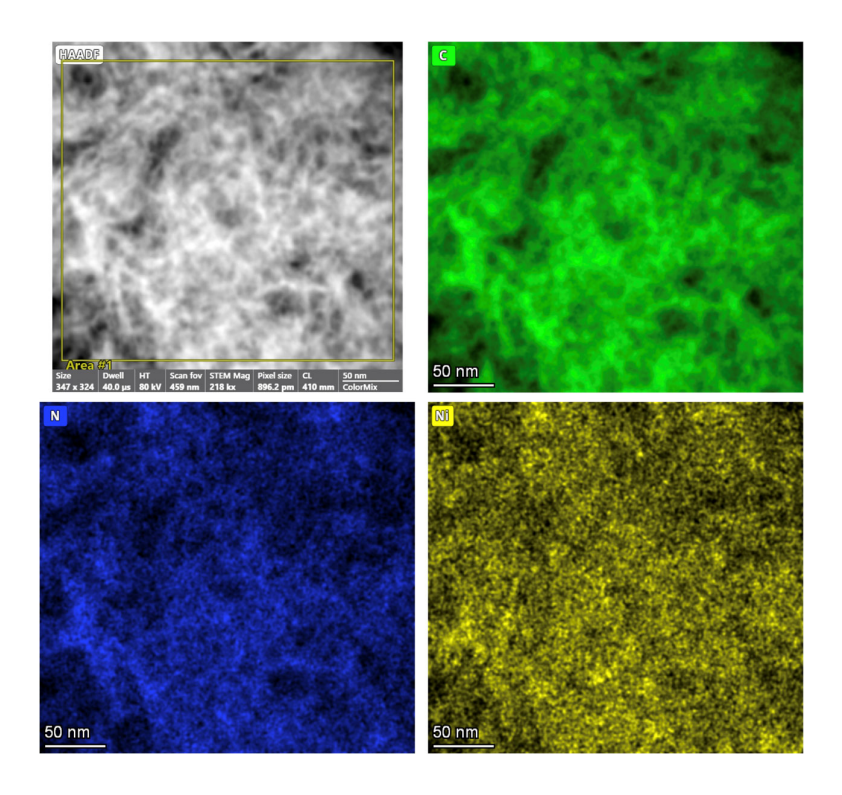
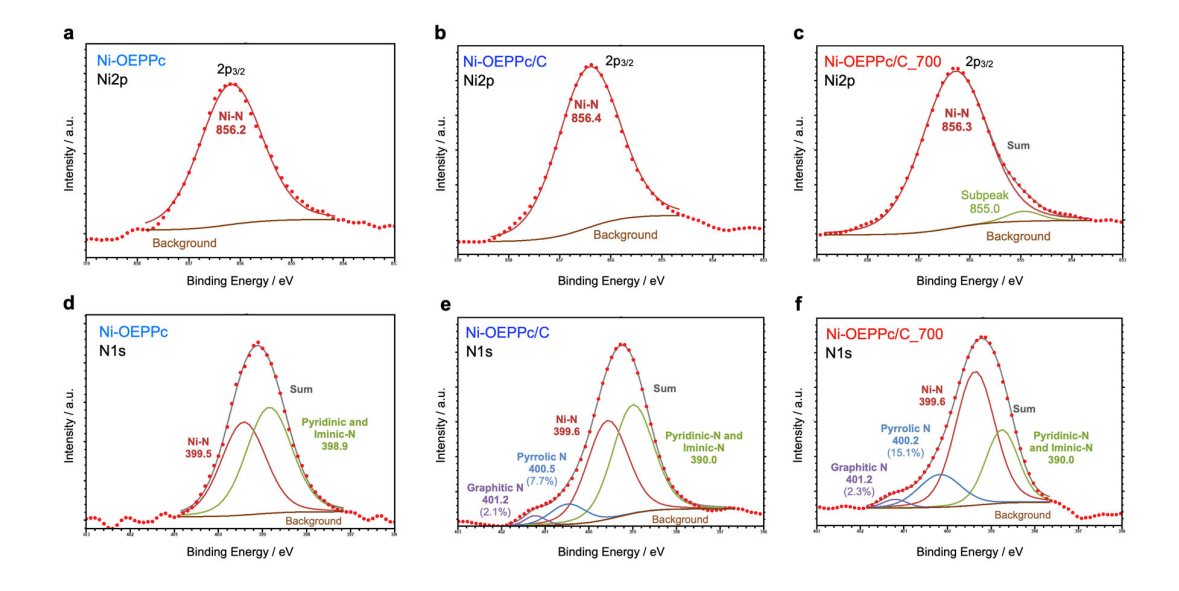


Fig. S25 Bright-field TEM image of Ni-OEPPc.



**Fig. S26** Representative HAADF-STEM image of **Ni-OEPPc/C** and corresponding EDX mapping of C, N, and Ni, respectively.



**Fig. S27** (a-c) Ni 2p<sub>3/2</sub> XP spectra of **Ni-OEPPc**, **Ni-OEPPc/C**, and **Ni-OEPPc/C\_700**. The subpeak observed in (c) is ascribed to the negligible amount of oxidized Ni species, carbides, or metallic Ni.<sup>7</sup> (d-f) N1s XP spectra of **Ni-OEPPc**, **Ni-OEPPc/C**, and **Ni-OEPPc/C\_700**.

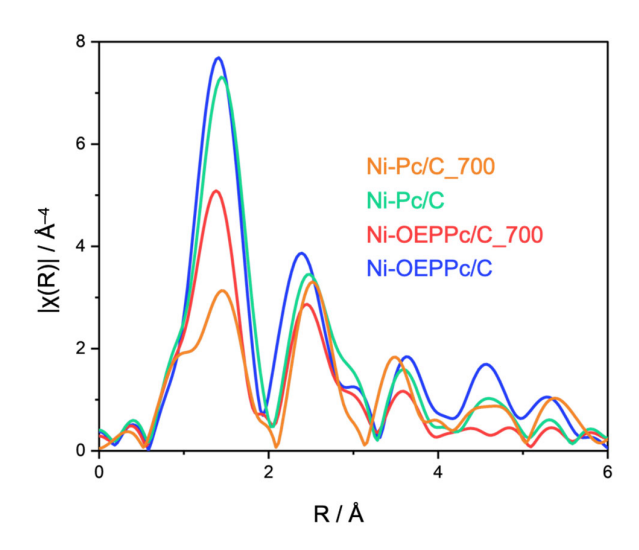


Fig. S28 EXAFS spectra of Ni-OEPPc/C\_700, Ni-OEPPc/C, Ni-Pc/C, and Ni-Pc/C\_700.

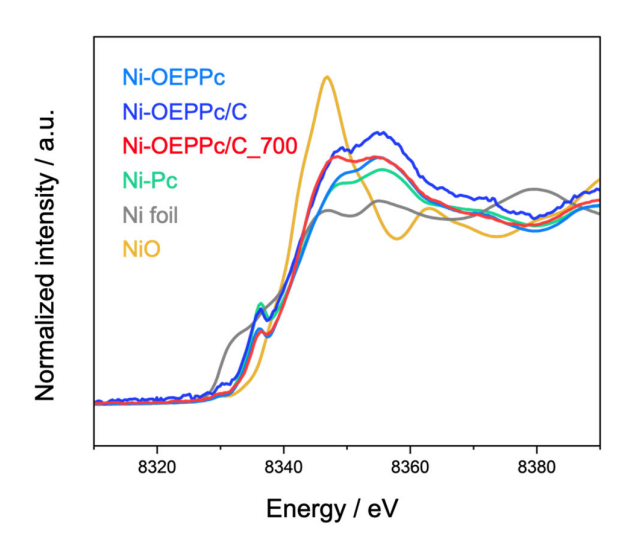


Fig. S29 XANES spectra of Ni-OEPPc, Ni-OEPPc/C, Ni-OEPPc/C\_700, Ni-Pc, Ni foil and NiO.

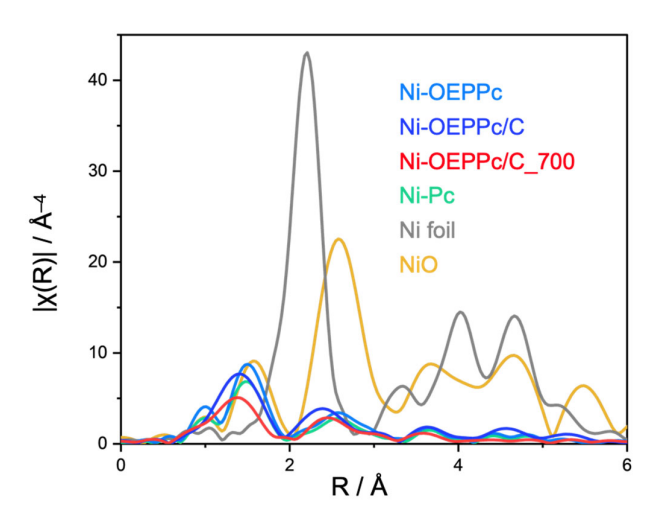


Fig. S30 EXAFS spectra of Ni-OEPPc, Ni-OEPPc/C, Ni-OEPPc/C\_700, Ni-Pc, Ni foil and NiO.

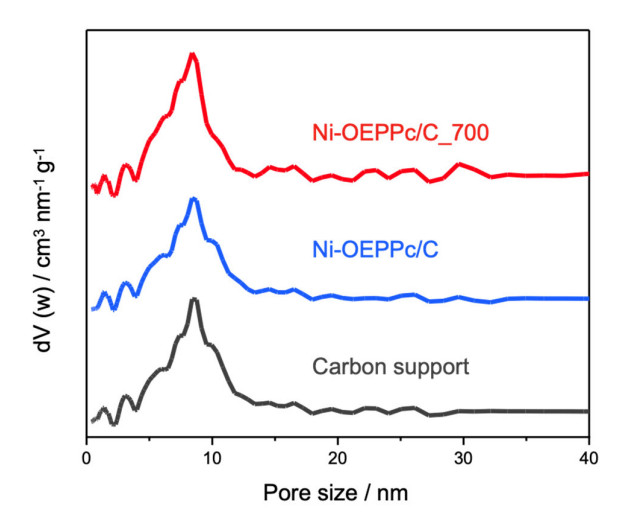


Fig. S31 Pore size distributions calculated using NLDFT method for Ni-OEPPc/C, Ni-OEPPc/C\_700, and the carbon support.

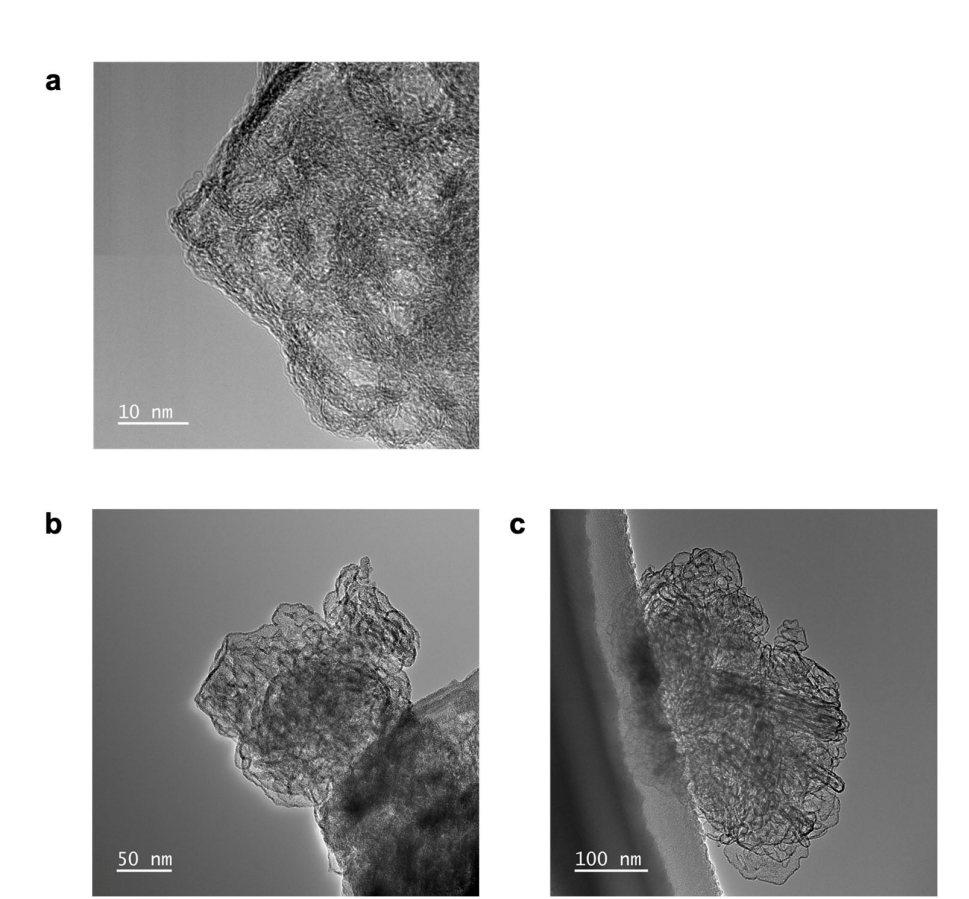


Fig. S32 TEM images of Ni-OEPPc/C\_700.

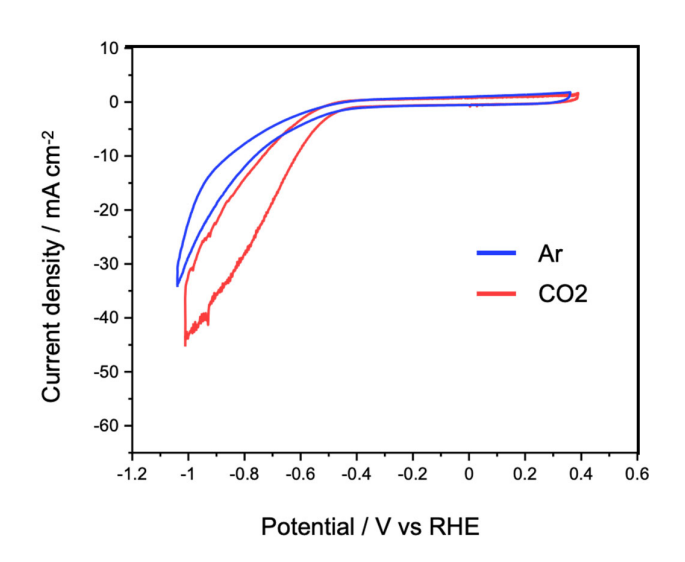


Fig. S33 Cyclic voltammograms of Ni-OEPPc/C\_700 in  $CO_2$ -saturated 1 M KHCO<sub>3</sub> and Arsaturated 1 M phosphate buffer solutions.

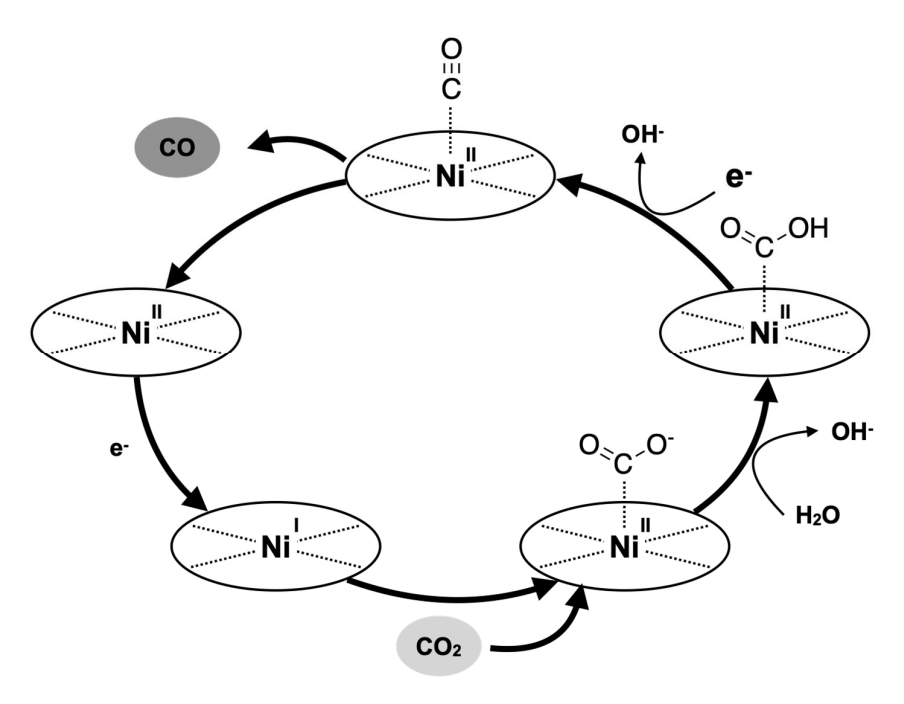


Fig. S34 Proposed reaction pathway for electrochemical  $CO_2$  reduction to CO over a Ni single-atom catalyst.<sup>8-11</sup>

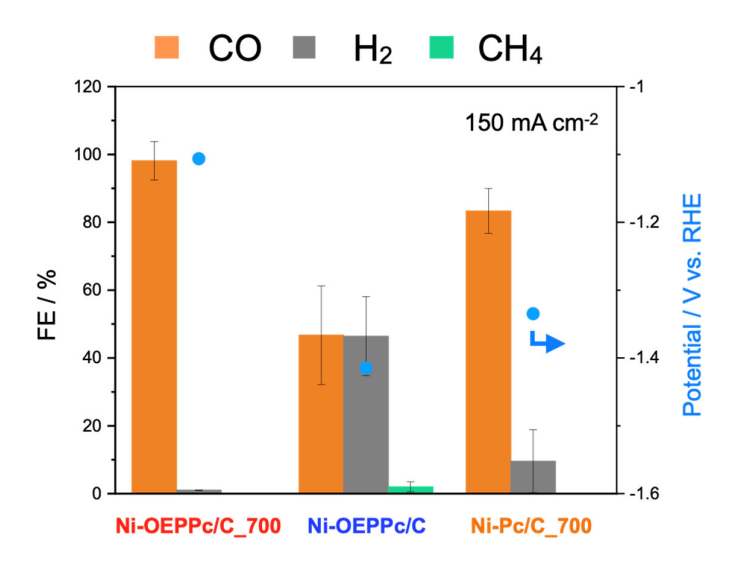


Fig. S35 Comparison of FE and potential during the reaction between Ni-OEPPc/C\_700, Ni-OEPPc/C, and Ni-Pc/C\_700.

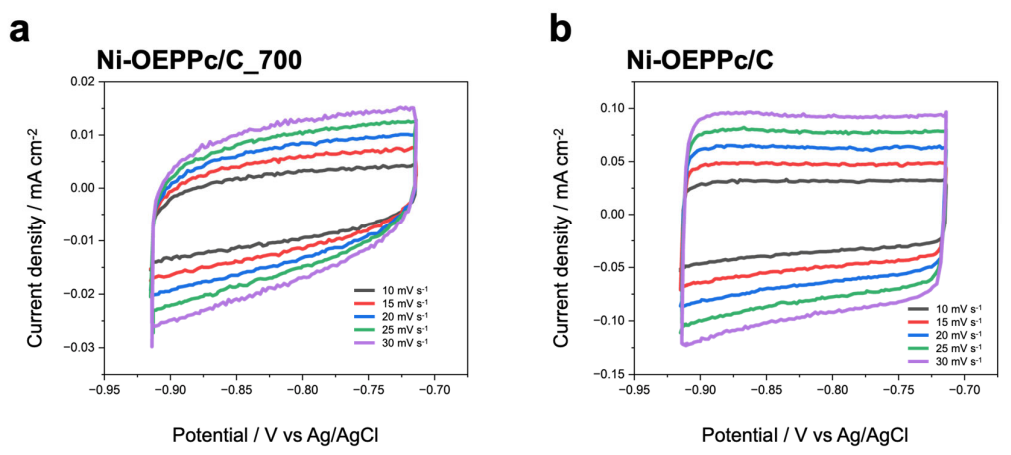
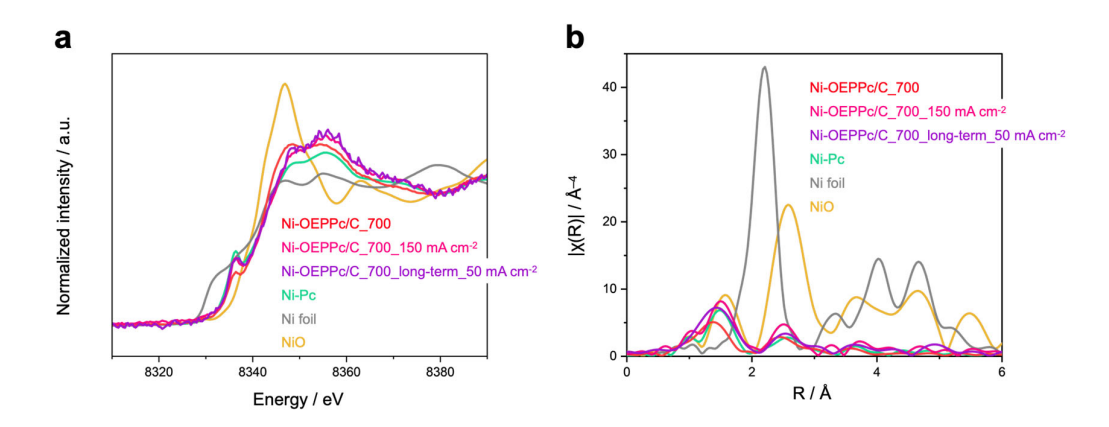


Fig. S36 Cyclic Voltammograms of Ni-OEPPc/C\_700 and Ni-OEPPc/C.



**Fig. S37** (a) XANES spectra of **Ni-OEPPc/C\_700** after electrolysis at 150 mA cm $^{-2}$  and 50 mA cm $^{-2}$  for 4h. (b) 30 spectra of **Ni-OEPPc/C\_700** after electrolysis at 150 mA cm $^{-2}$  and 50 mA cm $^{-2}$  for 4h.

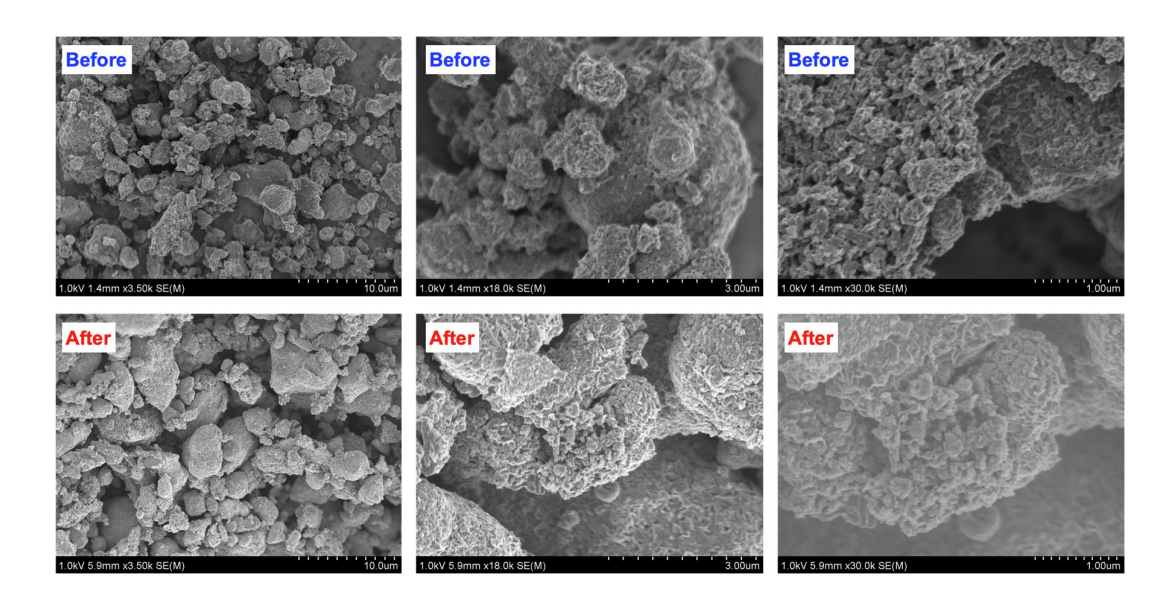


Fig. S38 SEM images of Ni-OEPPc/C\_700 before and after the  $CO_2RR$  operation. Ni-OEPPc/C\_700 was detached from GDE to conduct the SEM observation.

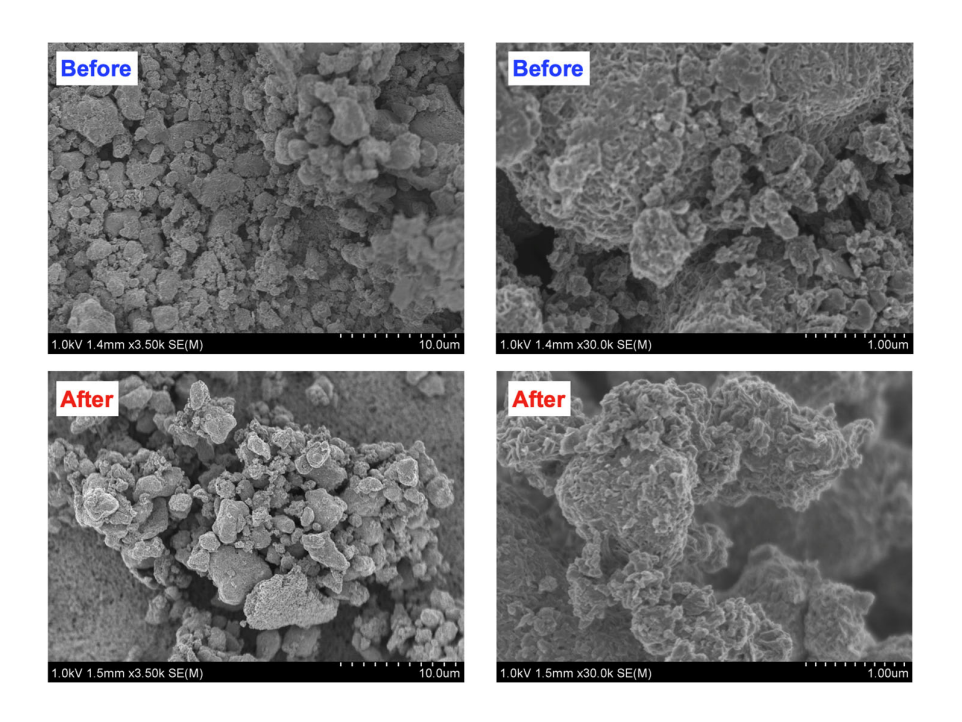
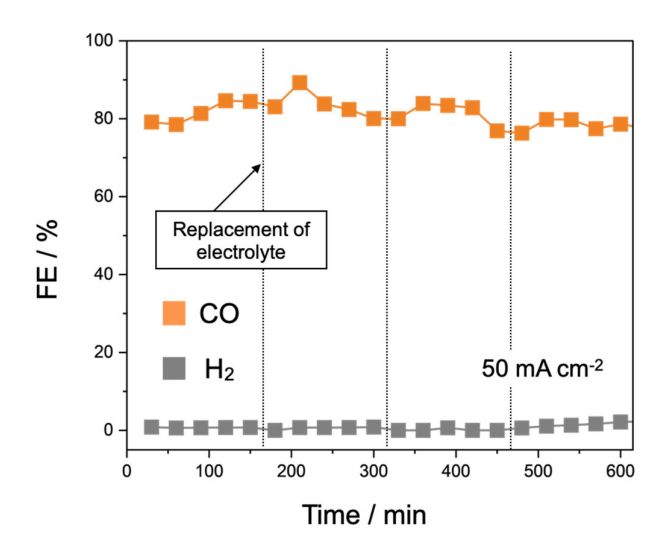
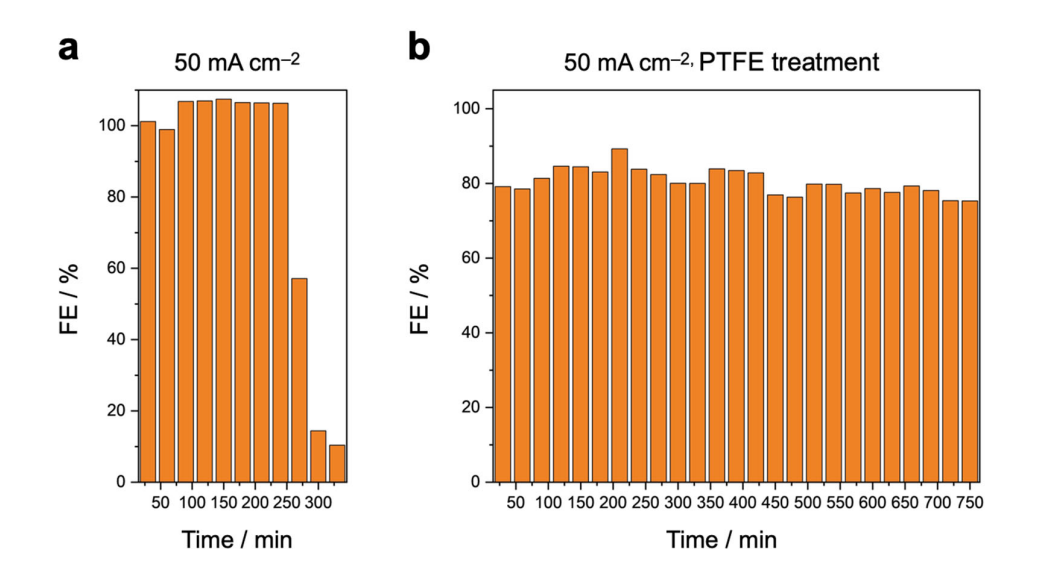


Fig. S39 SEM images of Ni-OEPPc/C\_700 before and after the  $CO_2RR$  operation. Ni-OEPPc/C\_700 on the GDE electrode was directly observed by SEM.



 $\textbf{Fig. S40} \ \ \text{Further long-term measurement of } \textbf{Ni-OEPPc/C\_700} \ \ \text{for 10 h at 50 mA cm}^{-2}.$ 



**Fig. S41** Faradaic efficiency for CO during long-term electrolysis using **Ni-OEPPc/C\_700**: (a) at 50 mA cm<sup>-2</sup> without PTFE treatment, (b) at 50 mA cm<sup>-2</sup> with PTFE treatment.

Table S1 Electrical conductivity of Ni-OEPPc, Ni-OEPPc\_250, Ni-OEPPc\_600, Ni-OEPPc\_700, and Ni-OEPPc\_800

|              | Electrical Conductivity (S/m) |
|--------------|-------------------------------|
| Ni-OEPPc     | 2×10 <sup>-8</sup>            |
| Ni-OEPPc_250 | 2×10 <sup>-8</sup>            |
| Ni-OEPPc_600 | 3×10 <sup>-3</sup>            |
| Ni-OEPPc_700 | 1.2×10⁻¹                      |
| Ni-OEPPc_800 | 3.5×10¹                       |

**Table S2** Ni K-edge EXAFS curve fitting parameters ( $S_0^2 = 0.83$ )

| Samples        | shell | CN  | R (Å) | $\sigma^2$ (Å <sup>2</sup> ) | R-factor |
|----------------|-------|-----|-------|------------------------------|----------|
| Ni foil        | Ni-Ni | 12* | 2.48  | 6.03×10 <sup>-3</sup>        | 0.001    |
| Ni-OEPPc_700   | Ni-N  | 4.1 | 1.88  | 3.52×10 <sup>-3</sup>        | 0.012    |
| Ni-OEPPc/C_700 | Ni-N  | 3.9 | 1.87  | 4.61×10 <sup>-3</sup>        | 0.008    |

CN, coordination number; R, bonding distance;  $\sigma^2$ , Debye-Waller factor;  $S_0^2$  was fixed to 0.83, according to the experimental EXAFS fit of Ni foil by fixing CN as the known crystallographic value. Fitting range:  $3 \le k$  (/Å)  $\le 11$  and  $1.0 \le R$  (Å)  $\le 3.0$  (Ni foil);  $2.0 \le k$  (/Å)  $\le 11$  and  $1.0 \le R$  (Å)  $\le 2.1$  (Ni-OEPPc\_700, Ni-OEPPc/C\_700).

Table S3 Faradaic efficiencies and the corresponding overpotentials of Ni-OEPPc/C\_700.

| Current density / mA cm <sup>-2</sup> | 10   | 50   | 100  | 150  | 200  |
|---------------------------------------|------|------|------|------|------|
| FEco / %                              | 83.9 | 87.6 | 92.9 | 98.0 | 65.4 |
| FE <sub>H2</sub> / %                  | 1.5  | 0.4  | 0.6  | 1.0  | 36.3 |
| Overpotential / V                     | 0.46 | 0.69 | 0.92 | 1.01 | 1.57 |

<sup>\*</sup>The overpotential was calculated using the equilibrium potentials shown below<sup>12</sup>.

$$CO_2 + 2H^+ + 2e^- \rightarrow CO_{(g)} + H_2O \qquad \qquad E^{eq} = \; -0.10 \; V \; vs \; RHE \label{eq:eq}$$

**Table S4** Summary of CO<sub>2</sub> reduction to CO by reported Ni-Pc-based catalysts<sup>13–24</sup>.

| Catalyst                        | Electrolyte   | FEco (%)      | Potential<br>(V vs. RHE) | j (mA cm <sup>-2</sup> ) | TOF*   | Mass activity<br>(mA mg <sup>-1</sup> ) | Ref.         |
|---------------------------------|---|---------------|--------------------------|--------------------------|--|---|--------------|
| Ni-OEPPc/CNo_700<br>(This work) | 1.0M KHCO₃  | 98            | -1.1                     | -150                     | 2.6 s <sup>-1</sup><br>(9360 h <sup>-1</sup> ) | 9.2×10³                                 | This<br>Work |
| HS-NiPc                         | 0.5 M KHCO₃   | 98.5          | -0.7                     | -2.7                     | 4097 h <sup>-1</sup>                           |   | 13           |
| NiPc                            | 0.5 M KHCO₃   | 99.1 (-0.9 V) | -1.1                     | -35                      | 3,772 h <sup>-1</sup>                          | 3.4×10³                                 | 14           |
| NiPc/KB                         | 0.5 M KHCO₃   | >90           | -1.05                    | -16.8                    | 11,475 h <sup>-1</sup>                         |   | 15           |
| NiPc-OMe/CNT                    | 0.5 M KHCO₃   | 99.1          | -0.61                    | -150                     | 12 s <sup>-1</sup>                             | 1.97×10 <sup>4</sup>                    | 16           |
| NiPc-G                          | 0.5 M KHCO₃   | 82.55         | -0.83                    | -20.4                    | 6089 h <sup>-1</sup>                           |   | 17           |
| NiPc-CNT-20                     | 0.5 M KHCO₃   | 98.82         | -0.83                    | -9.1                     | 2110 h <sup>-1</sup>                           |   | 17           |
| NiPc-OMe/CNT                    | 0.1 M H <sub>2</sub> SO <sub>4</sub> + 0.4 M K <sub>2</sub> SO <sub>4</sub> | >99           | -1.26                    | -100                     |  | 1.28×10 <sup>4</sup>                    | 18           |
| NiPc/CF                         | 0.5 M KHCO₃   | 98.9          | -0.8                     | -6.7                     |  |   | 19           |
| NiPc-NiO <sub>4</sub>           | 0.5 M KHCO₃   | 98.4          | -1.2                     | -34.3                    | 2603 h <sup>-1</sup>                           |   | 20           |
| NiTAPc/CNT                      | 1.0 M KHCO₃   | 99.9          |                          | -150                     |  | 4.32×10 <sup>4</sup>                    | 21           |
| Ni-CNT-CC                       | 0.5 M KHCO₃   | 99            | -0.6                     | -32.2                    | 100179 h <sup>-1</sup>                         | 1.19×10⁵                                | 22           |
| NiPc(OH) <sub>6</sub> (DCNFO)   | 0.5 M KHCO₃   | 98            | -0.9                     | -140                     |  |   | 23           |
| NiPc-B/CNT                      | 1.0 M KHCO₃   | >99           | -0.67                    | -150                     | 13.77 s <sup>-1</sup>                          | 4.55×10 <sup>4</sup>                    | 24           |

<sup>\*</sup>TOF Turnover efficiency

**Table S5** Summary of CO<sub>2</sub>RR performances of pyrolyzed NiPc-derived materials<sup>25–31</sup>.

| Catalyst                        | Electrolyte             | FEco (%) | Potential<br>(V vs. RHE) | j (mA cm <sup>-2</sup> ) | TOF  | Mass activity<br>(mA mg <sup>-1</sup> ) | Ref. |
|---------------------------------|-------------------------|----------|--------------------------|--------------------------|--|---|------|
| Ni-OEPPc/CNo_700<br>(This work) | 1.0M KHCO₃              | 98       | -1.1                     | -150                     | 2.6 s <sup>-1</sup><br>(9360 h <sup>-1</sup> ) | 9.2×10³                                 |      |
| Ni-SAC                          | 1.0 M KHCO <sub>3</sub> | 96       | -0.7                     | -192                     |  | 8.73×10 <sup>3</sup>                    | 25   |
| Ni-BMBC                         | 0.5 M KHCO₃             | 86       | -1.0                     | -96                      |  | 1.02×10 <sup>4</sup>                    | 26   |
| Ni-NHCS                         | 0.5 M NaHCO₃            | 98.57    | -0.87                    | -14.2                    | 3.75 s <sup>-1</sup>                           |   | 27   |
| Ni-PPc                          | 0.5 M KHCO₃             | 98.2     | -0.7                     | -15.0                    | 1.36 s <sup>-1</sup>                           |   | 28   |
| Ni SA/NHCR                      | 1.0 M KHCO₃             | 98.41    | -0.8                     | -100                     |  |   | 29   |
| H-NiPc/CNT                      | 0.5 M KHCO₃             | >90      | -0.94                    | -17                      | 13,860 h <sup>-1</sup>                         |   | 30   |
| Ni-NCI                          | 0.5 M KHCO₃             | 98       | -0.98                    | -57.5                    | >6000 h <sup>-1</sup>                          |   | 31   |

**Table S6** Summary of  $CO_2RR$  performances of Ni-SAC catalysts (excluding Ni-Pc-derived materials)<sup>33–39</sup>.

| Catalyst                             | Electrolyte | FEco (%) | Potential<br>(V vs. RHE) | j (mA cm <sup>-2</sup> ) | TOF  | Mass activity<br>(mA mg <sup>-1</sup> ) | Ref. |
|--------------------------------------|-------------|----------|--------------------------|--------------------------|--|---|------|
| Ni-OEPPc/CNo_700<br>(This work)      | 1.0M KHCO₃  | 98       | -1.1                     | -150                     | 2.6 s <sup>-1</sup><br>(9360 h <sup>-1</sup> ) | 9.2×10³                                 |      |
| Ni-NCB                               | 0.1 M KHCO₃ | ≒100     |                          | -73.8                    | 6.36 s <sup>-1</sup>                           |   | 33   |
| Ni-N-HCNs-5h                         | 1.0 M KOH   | 96       | -1.17                    | -577.4                   |  | 6.75×10 <sup>4</sup>                    | 34   |
| Ni@C <sub>3</sub> N <sub>4</sub> -CN | 1.0 M KHCO₃ | 90       | -0.93                    | -300                     | 22,000 h <sup>-1</sup>                         | 1.39×10⁵                                | 35   |
| NiSA/PCFM                            | 0.5 M KHCO₃ | 88       | -1.0                     | -308.4                   |  | 3.63×10 <sup>4</sup>                    | 36   |
| Ni SAs-NCW                           | 1.0 M KOH   | 60       | -1.16                    | -74.5                    | 894 h <sup>-1</sup>                            |   | 37   |
| Ni (NC)-1                            | 1.0 M KOH   | 99       | -1.82                    | -160                     |  |   | 38   |
| Ni-N-C                               | 1.0 M KHCO₃ | 85       | -1.0                     | -200                     |  | 2.0×10 <sup>3</sup>                     | 39   |

Table S7 Mass specific ECSA and specific activity of Ni-OEPPc/C\_700 and Ni-OEPPc/C.

| Sample  | Ni-OEPPc/C_700       |                      | Ni-OEPPc/C_700       |                      | Ni-OE | PPc/C |
|---|----------------------|----------------------|----------------------|----------------------|-------|-------|
| Mass specific ECSA (cm <sup>2</sup> g <sup>-1</sup> ) | 30.8                 |                      | 213                  | 3.5                  |       |       |
| Current density(mA cm <sup>-2</sup> )                 | 10                   | 150                  | 10                   | 150                  |       |       |
| Specific activity (A g <sup>-1</sup> )                | 1.5×10 <sup>-3</sup> | 2.6×10 <sup>-2</sup> | 2.2×10 <sup>-4</sup> | 2.5×10 <sup>-3</sup> |       |       |

Table S8 Comparison of FE among Ni-OEPPc/C\_700, Ni-OEPPc/C, Ni-OEPPc\_700, and Ni-OEPPc.

| Catalyst             | Ni-OEPPc/C_700 | Ni-OEPPc_700 | Ni-OEPPc_700/C |
|----------------------|----------------|--------------|----------------|
| Temp / °C            | 700            | 700          | 700            |
| FEco/%               | 84             | 10           | 23             |
| FE <sub>H2</sub> / % | 1              | 86           | 69             |

**Table S9** Faraday efficiencies for formic acid formation over **Ni-OEPPc/C\_700** at current densities of 10, 50, 100, 150, and 200 mA cm<sup>-2</sup>.

| Current density / mA cm <sup>-2</sup> | FE <sub>HCOOH</sub> / % |
|---------------------------------------|-------------------------|
| 10                                    | n.d.                    |
| 50                                    | 0.1                     |
| 100                                   | 0.1                     |
| 150                                   | 0.1                     |
| 200                                   | 1.7                     |

**Table S10** Time-courses of FEco and FE<sub>H2</sub> for **Ni-OEPPc/C\_700** at 50 mA cm<sup>-2</sup>.

| Time / min           | 30    | 60   | 90    | 120   | 150   | 180   | 210   | 240   |
|----------------------|-------|------|-------|-------|-------|-------|-------|-------|
| FEco/%               | 101.1 | 98.9 | 106.8 | 106.7 | 107.5 | 106.5 | 106.4 | 106.3 |
| FE <sub>H2</sub> / % | 0.5   | 0.7  | 0.9   | 1.1   | 1.2   | 1.4   | 2.3   | 3.0   |

## Reference for ESI

- 1 Wagner CD, Naumkin AV, Vass AK, et al. NIST Standard Reference Database 20, Version 3.4 (web version) (http://srdata.nist.gov/xps/), 2003
- 2 M. Inagaki, M. Toyoda, Y. Soneda and T. Morishita, Carbon, 2018, 132, 104–140.
- 3 A. Casotto, G. Drera, D. Perilli, S. Freddi, S. Pagliara, M. Zanotti, L. Schio, A. Verdini, L. Floreano, C. D. Valentin and L. Sangaletti, *Nanoscale*, 2022, **14**, 13166–13177.
- 4 B. Ravel and M. Newville, J. Synchrotron Rad., 2005, 12, 537–541.
- 5 P. Grabowska, M. Szkoda, M. Skorupska, J. P. Lukaszewicz and A. Ilnicka, *Sci Rep*, 2023, **13**, 18632.
- 6 J. Su, Y. Liu, N. Jiang, B. Jiang, Y. Wang, X. Wang, Y. Chen and H. Song, J. Alloys Compd., 2024, 970, 172287.
- 7 I. Czekaj, F. Loviat, F. Raimondi, J. Wambach, S. Biollaz and A. Wokaun, *Appl. Catal. A: Gen.*, 2007, **329**, 68–78.
- Z. Zhang, J. Xiao, X.-J. Chen, S. Yu, L. Yu, R. Si, Y. Wang, S. Wang, X. Meng, Y. Wang,
  Z.-Q. Tian and D. Deng, *Angew. Chem. Int. Ed.*, 2018, 57, 16339–16342.
- M. Zhu, R. Ye, K. Jin, N. Lazouski and K. Manthiram, ACS Energy Lett., 2018, 3, 1381– 1386.
- Q. Chang, Y. Liu, J.-H. Lee, D. Ologunagba, S. Hwang, Z. Xie, S. Kattel, J. H. Lee and J. G. Chen, *J. Am. Chem. Soc.*, 2022, **144**, 16131–16138.
- 11 M. Li, H. Wang, W. Luo, P. C. Sherrell, J. Chen and J. Yang, *Adv. Mater.*, 2020, **32**, 2001848.
- 12 S. Nitopi, E. Bertheussen, S. B. Scott, X. Liu, A. K. Engstfeld, S. Horch, B. Seger, I. E. L. Stephens, K. Chan, C. Hahn, J. K. Nørskov, T. F. Jaramillo and I. Chorkendorff, *Chem. Rev.*, 2019, **119**, 7610–7672.
- 13 X. Wang, Y. Fu, D. Tranca, K. Jiang, J. Zhu, J. Zhang, S. Han, C. Ke, C. Lu and X. Zhuang, *ACS Appl. Energy Mater.*, 2021, **4**, 2891–2898.
- 14 M.-D. Zhang, D.-H. Si, J.-D. Yi, S.-S. Zhao, Y.-B. Huang and R. Cao, *Small*, 2020, **16**, 2005254.
- 15 Z. Ma, X. Zhang, X. Han, D. Wu, H. Wang, Z. Gao, F. Xu and K. Jiang, *Appl. Surf. Sci.*, 2021, **538**, 148134.
- 16 X. Zhang, Y. Wang, M. Gu, M. Wang, Z. Zhang, W. Pan, Z. Jiang, H. Zheng, M. Lucero, H. Wang, G. E. Sterbinsky, Q. Ma, Y.-G. Wang, Z. Feng, J. Li, H. Dai and Y. Liang, *Nat. Energy*, 2020, 5, 684–692.
- 17 C. Guo, S. Liu, Z. Chen, B. Li, L. Chen, C. V. Singh, B. Liu and Q. Mao, *Chem. Commun.*, 2021, **57**, 1384–1387.
- 18 Z. Jiang, Z. Zhang, H. Li, Y. Tang, Y. Yuan, J. Zao, H. Zheng and Y. Liang, Adv. Energy

- *Mater.*, 2023, **13**, 2203603.
- 19 Z. Zhu, G. Yu, L. Duan, X. Liu, L. Wang and J. Zhang, J. Mol. Liq., 2023, 376, 121432.
- 20 J.-D. Yi, D.-H. Si, R. Xie, Q. Yin, M.-D. Zhang, Q. Wu, G.-L. Chai, Y.-B. Huang and R. Cao, *Angew. Chem. Int. Ed.*, 2021, **60**, 17108–17114.
- 21 K. Chen, M. Cao, Y. Lin, J. Fu, H. Liao, Y. Zhou, H. Li, X. Qiu, J. Hu, X. Zheng, M. Shakouri, Q. Xiao, Y. Hu, J. Li, J. Liu, E. Cortés and M. Liu, Adv. Funct. Mater., 2022, 32, 2111322.
- 22 S. Liu, H. B. Yang, S.-F. Hung, J. Ding, W. Cai, L. Liu, J. Gao, X. Li, X. Ren, Z. Kuang, Y. Huang, T. Zhang and B. Liu, *Angew. Chem. Int. Ed.*, 2020, **59**, 798–803.
- 23 Y. Jin, X. Zhan, Y. Zheng, H. Wang, X. Liu, B. Yu, X. Ding, T. Zheng, K. Wang, D. Qi and J. Jiang, *Appl. Catal. B: Environ.*, 2023, **327**, 122446.
- 24 Y. Huang, H. Dai, D. Moonshiram, Z. Li, Z.-M. Luo, J.-H. Zhang, W. Yang, Y. Shen, J.-W. Wang and G. Ouyang, *J. Mater. Chem. A*, 2023, 11, 2969–2978.
- 25 Y. Wang, Z. Jiang, X. Zhang, Z. Niu, Q. Zhou, X. Wang, H. Li, Z. Lin, H. Zheng and Y. Liang, ACS Appl. Mater. Interfaces, 2020, 12, 33795–33802.
- 26 K. Hu, S. Jia, B. Shen, Z. Wang, Z. Dong and H. Lyu, Chem. Eng. J., 2024, 497, 154686.
- 27 S. Gong, W. Wang, R. Lu, M. Zhu, H. Wang, Y. Zhang, J. Xie, C. Wu, J. Liu, M. Li, S. Shao, G. Zhu and X. Lv, *Appl. Catal. B: Environ.*, 2022, **318**, 121813.
- 28 J. Chen, J. Li, J. Xu, M. Zhu and Y.-F. Han, Green Energy Environ., 2023, 8, 444–451.
- 29 S. Gong, S. Yang, W. Wang, R. Lu, H. Wang, X. Han, G. Wang, J. Xie, D. Rao, C. Wu, J. Liu, S. Shao and X. Lv, Small, 2023, 19, 2207808.
- 30 Y. J. Sa, H. Jung, D. Shin, H. Y. Jeong, S. Ringe, H. Kim, Y. J. Hwang and S. H. Joo, *ACS Catal.*, 2020, **10**, 10920–10931.
- 31 S.-M. Wang, X. Yuan, S. Zhou, X. Li, S.-G. Han, W. Lin, L. Zheng, D.-D. Ma and Q.-L. Zhu, *Energy Mater.*, 2024, **4**, 400032.
- 32 J.-H. Wu, J.-W. Wang, B. M. Aramburu-Trošelj, F.-J. Niu, L.-J. Guo and G. Ouyang, *Nanoscale*, 2024, **16**, 11496–11512.
- 33 T. Zheng, K. Jiang, N. Ta, Y. Hu, J. Zeng, J. Liu and H. Wang, Joule, 2019, 3, 265–278.
- 34 Z. Liu, L. Cao, M. Wang, Y. Zhao, M. Hou and Z. Shao, *J. Mater. Chem. A*, 2024, **12**, 8331–8339.
- 35 Q. Wang, K. Liu, K. Hu, C. Cai, H. Li, H. Li, M. Herran, Y.-R. Lu, T.-S. Chan, C. Ma, J. Fu, S. Zhang, Y. Liang, E. Cortés and M. Liu, *Nat. Commun.*, 2022, **13**, 6082.
- 36 H. Yang, Q. Lin, C. Zhang, X. Yu, Z. Cheng, G. Li, Q. Hu, X. Ren, Q. Zhang, J. Liu and C. He, *Nat Commun*, 2020, 11, 593.
- 37 H. Chang, H. Pan, F. Wang, Z. Zhang, Y. Kang and S. Min, *Nanoscale*, 2022, **14**, 10003–10008.
- 38 C. F. Wen, F. Mao, Y. Liu, X. Y. Zhang, H. Q. Fu, L. R. Zheng, P. F. Liu and H. G. Yang,

ACS Catal., 2020, 10, 1086-1093.

39 T. Möller, W. Ju, A. Bagger, X. Wang, F. Luo, T. N. Thanh, A. S. Varela, J. Rossmeisl and P. Strasser, *Energy Environ. Sci.*, 2019, **12**, 640–647.